Canadian Geotechnical Journal

Research Article

Unified frameworks for modeling small-strain stiffness and critical state behavior in gap-graded soils

Deyun Liu[a], **Jidong Zhao**[b], **Shijin Feng**[a,c], **and Duan Yang**[a]

[a]Department of Geotechnical Engineering, Tongji University, Shanghai 200092, China; [b]Department of Civil & Environmental Engineering, The Hong Kong University of Science and Technology, Hong Kong, China; [c]Key Laboratory of Geotechnical and Underground Engineering of the Ministry of Education, Tongji University, Shanghai 200092, China

Corresponding authors: **Jidong Zhao** (email: jzhao@ust.hk); **Shijin Feng** (email: fsjgly@tongji.edu.cn)

Abstract

This study employs the discrete element method to investigate the mechanical behavior of gap-graded soils across a wide range of strain levels, explicitly accounting for particle property variability at the particle scale. The analyses reveal that the stress-transmission role of finer particles is primarily governed by finer fraction, density, and strain level, contributing more strongly to mean effective stress than to deviatoric stress. Although their transmission efficiency increases with finer fraction and density, finer particles remain less effective than coarse particles in transferring stress. These nonequivalent mechanical contributions highlight the limitation of conventional state variables, such as void ratio, skeleton void ratio, mechanical void ratio, and the state parameter, which fail to capture the evolving roles of coarse and finer particles. A micromechanically calibrated refinement is therefore proposed, incorporating the partial stress contributions of finer particles and linking small-strain stiffness and critical state behavior within a unified framework. The refined variable successfully reproduces both small-strain and critical state responses for mixtures with up to 50% finer fraction. Overall, the findings clarify the micromechanical mechanisms governing stress transmission and structure evolution in gap-graded soils, providing a physically grounded basis for potential practical engineering.

Key words: discrete element method, gap-graded soils, small-strain stiffness, critical states, state variables

Résumé

Cette étude utilise la méthode des éléments discrets pour étudier le comportement mécanique des sols à granulométrie discontinue sur une large gamme de niveaux de déformation, en tenant explicitement compte de la variabilité des propriétés des particules à l'échelle particulaire. Les analyses révèlent que le rôle des particules fines dans la transmission des contraintes est principalement régi par la fraction fine, la densité et le niveau de déformation, leur contribution étant plus importante à la contrainte effective moyenne qu'à la contrainte déviatorique. Bien que leur efficacité de transmission augmente avec la fraction fine et la densité, les particules fines demeurent moins efficaces que les particules grossières pour transférer les contraintes. Ces contributions mécaniques non équivalentes soulignent les limites des variables d'état conventionnelles, telles que l'indice des vides, l'indice des vides du squelette, l'indice des vides mécanique et le paramètre d'état, qui ne parviennent pas à rendre compte de l'évolution des rôles des particules grossières et fines. Un raffinement, calibré à l'échelle micromécanique, de la formulation de Thevanayagam (2000) est donc proposé. Il intègre les contributions partielles des particules fines à la transmission des contraintes et établit un lien entre la rigidité aux faibles déformations et le comportement à l'état critique dans un cadre unifié. La variable raffinée reproduit avec succès les réponses aux faibles déformations et à l'état critique pour des mélanges contenant jusqu'à 50 % de fraction fine. Dans l'ensemble, les résultats clarifient les mécanismes micromécaniques régissant la transmission des contraintes et l'évolution de la structure dans les sols à granulométrie discontinue, fournissant une base physiquement fondée pour de potentielles applications pratiques en ingénierie.

Mots-clés : méthode des éléments discrets, sols à granulométrie discontinue, rigidité aux faibles déformations, états critiques, variables d'état

1. Introduction

Silty sands, also known as gap-graded soils, are mixtures of coarse and finer particles commonly found in regions shaped by fluvial or glacial processes. In alluvial and deltaic environments, the differential transport and deposition of particles of varying sizes contribute to the formation of these soils (e.g., Allen 1965; Church 2006). The presence of gap-graded soils can lead to geotechnical hazards, including internal erosion due to suffusion effects (e.g., Liang et al. 2017; Hu et al. 2020) and an increased susceptibility to liquefaction under dynamic conditions (e.g., Chang et al. 2014; Chitravel et al. 2023). A significant challenge with gap-graded soils is that their behavior does not always conform to conventional soil behavior frameworks. This divergence has prompted extensive research for gap-graded soils over the past two decades (e.g., Lade and Yamamuro 1997; Salgado et al. 2000; Thevanayagam et al. 2002; Ni et al. 2004; Murthy et al. 2007; Rahman et al. 2008; Carraro et al. 2009; Yang and Liu 2016; Otsubo et al. 2021; Deyun et al. 2022; Wang et al. 2023; Liu et al. 2024*a*).

There is a general consensus that the behavior of gap-graded soils is closely related to the mass proportion of the finer fraction, denoted as F_{finer}. Previous studies have acknowledged that the conventional state variable—the global void ratio (e)—is inadequate for describing the behavior of gap-graded soils (Mitchell and Soga 1976), since a significant portion of finer particles may remain inactive in stress transmission. Consequently, Shen (1977) introduced the skeleton void ratio (e_s), treating all finer particles as part of the void space. While Thevanayagam (2000), Ni et al. (2004), and Rahman et al. (2008) argued that the potential contribution of finer particles should be taken into account as F_{finer} increases, they proposed various equivalent void ratios based on purely empirical formulations. However, divergent views have emerged regarding the appropriate selection of state variables (e.g., Carrera et al. 2011; Yang et al. 2015). Specifically, Yang et al. (2018) emphasized that neither the global void ratio nor the equivalent void ratio effectively captures the behavior of gap-graded soils; instead, they advocated for state parameters derived from critical state to better represent the small-strain stiffness behavior of gap-graded soils in a unified manner. The main reason for these contrasting perspectives lies in the ambiguous role of finer particles, which is challenging, if not impossible, to quantify accurately in conventional experimental studies. This ambiguity further results in insufficient explanatory mechanisms for estimating these proposed state variables.

Leveraging advancements in computational capabilities, numerical methods—particularly the discrete element method (DEM)—have become powerful tools for investigating the behavior of gap-graded soils. DEM facilitates a detailed examination of individual particle interactions (e.g., Chang and Yin 2011; Shire et al. 2014; Zhao et al. 2018; Ahmadi et al. 2020; Otsubo et al. 2021; Liu et al. 2024*b*; Song et al. 2024*b*; Wang et al. 2024). Although the models employed in these studies are often idealized, they offer the significant advantage of enabling analysis of particle stress and contact force data. This capability allows for an in-depth study of the role of finer particles in gap-graded soils, encompassing aspects such as particle stress transmission (e.g., Shire et al. 2014), small-strain stiffness (G_0) (Gong et al. 2019*b*; Liu et al. 2022*b*), and shearing behavior (e.g., Sufian et al. 2021; Adesina et al. 2024).

Recent studies have also proposed alternative state variables to better describe the behavior of gap-graded soils. For instance, Otsubo (2016) introduced a mechanical void ratio (e_m), defined as $e_m = (V_v + V_{iac})/V_a$, where V_v is the volume of voids, V_{iac} represents the volume of inactive particles, and V_a is the volume of active particles. Inactive particles are those with one or zero contact points, rendering them incapable of transferring stress. Sufian et al. (2021) demonstrated that the roles of active coarse and finer particles can also be distinct during shearing, suggesting that e_m may not adequately capture the behavior of gap-graded soils. Consequently, they proposed a semi-empirical granular void ratio (e_G), which employs a minor threshold stress level to differentiate active particles from inactive ones, considering finer particles transferring limited stress as inactive. While their method shows improved performance in modeling the behavior of gap-graded soils, it remains empirical without a rational underlying mechanism.

Additionally, due to the high computational demands of studying gap-graded soils using DEM, there are limited studies that shear specimens to critical states. The simulations configurations for gap-graded soils could be more rigorous. For instance, Sufian et al. (2021) stated that to maintain steady and stable shearing behavior, specimens should be sufficiently large, with a minimum coarse particle count of approximately 500. Furthermore, the shearing rate should be selected maintaining an inertia number of $I < 1 \times 10^{-6}$ (Da Cruz et al. 2005) to ensure quasi-static conditions. Here, $I = \dot{\varepsilon} d_{50}\sqrt{\rho/p'}$, where $\dot{\varepsilon}$ is the strain rate, d_{50} is the median particle diameter, ρ is particle density (2670 kg/m^3 for coarse and finer particles), and p' is the effective confining pressure. However, the maximum axial strain demonstrated in Sufian et al. (2021) was only 5%, indicating a lack of quantification on critical state of gap-graded soils. Besides, it remains unclear whether the state parameters determined at the critical state can effectively describe the small-strain stiffness characteristics of gap-graded soils (Yang et al. 2018).

Another significant issue is that nearly all these studies assume that the particle properties of both coarse and finer particles are identical, which may not reflect the realities of natural environments. Natural gap-graded soils can be found in alluvial fans, colluvial deposits, and residual soils, where particles display distinct properties. For instance, gap-graded soils can form at the junction of two rivers with different sedimentary histories and environmental conditions, resulting in particles with varying characteristics. Recognizing this natural variability is essential for achieving accurate and safe outcomes in engineering practices (e.g., Tian and Senetakis 2022, 2024; Liu and Lyu 2023, 2024), and prior experimental studies have demonstrated great variability in particle properties (Sandeep and Senetakis 2018; Liu et al. 2019*b*; Nardelli and Coop 2019).

Therefore, this study aims to (1) incorporate the potential variability of particle-scale mechanical parameters to provide a more realistic representation of the inherent heterogeneity in gap-graded soils; (2) evaluate existing state variables to examine their capability in linking small-strain and critical state behaviors, revealing their applicability in capturing the evolving role of fines across different densities and gradations; (3) refine existing state variables to better capture the distinct mechanical contributions of coarse and finer particles, extending their applicability from small-strain to large-strain regimes approaching the critical state.

2. Numerical simulation approach

The DEM simulations were performed using a modified version code of LAMMPS code (Thompson et al. 2022). In DEM, these grains are modeled as rigid bodies with overlap to simulate real particle deformation. The method computes contact forces at each time-step. Specifically, contacts were modeled with the Hertz–Mindlin formulation implemented via Pair_style granular in LAMMPS, using the material-based normal law (hertz/material) and a history-dependent tangential law (mindlin_rescale/force). The normal force ($\boldsymbol{F}_{\mathrm{n}}$) follows the Hertz relation:

$$\boldsymbol{F}_{\mathrm{n}} = \frac{4}{3}E_{\mathrm{eff}}R_{\mathrm{eff}}^{1/2}\delta_{\mathrm{ij}}^{3/2}\mathrm{n} \tag{1}$$

Here, $\delta_{ij} = R_i + R_j - \| \boldsymbol{r_{ij}} \|$ is the particle overlap, R_i, R_j are the particle radii, $\boldsymbol{r}_{ij} = r_i - r_j$ is the vector separating the two particle centers (note the *i–j* ordering so that F_n is positive for repulsion), and $\mathrm{n}=\frac{r_{ij}}{\|r_{ij}\|}$. $R_{\mathrm{eff}} = \frac{R_iR_j}{R_i+R_j}$ is the effective radius also presented as R, $E_{\mathrm{eff}} = \left(\frac{1-v_i^2}{E_i} + \frac{1-v_j^2}{E_j}\right)^{-1}$ is the effective Young's modulus also presented as E, with v_i, v_j the Poisson ratios of the particles of type *i* and *j*. For tangential contact model, the model of Mindlin_rescale/force is employed,

$$\mathrm{F_t} = -\min\left(\mu_t F_{n0,} \| - k_t a\xi \|\right)\mathrm{t} \tag{2}$$

Here, a is the radius of the contact region, given by $a = \sqrt{R\delta}$ for the normal contact model, where it is given implicitly by $\delta = a^2/R - 2\sqrt{\pi\gamma a/E}$. It can be seen that tangential friction also used a Coulomb limit with type-dependent inter-particle friction coefficient (μ) values. Besides, one should set $k_t = 8G_{\mathrm{eff}}$, where G_{eff} is the effective shear modulus given by

$$G_{\mathrm{eff}} = \left(\frac{2-v_i}{G_i} + \frac{2-v_j}{G_j}\right)^{-1} \tag{3}$$

where G_i is the shear modulus of a particle of type i, related to Young's modulus E_i and Poisson's ratio v_i by $G_i = E_i/(2/(1 + v_i))$.

While particle shape is known to significantly affect soil behavior (e.g., Zhao et al. 2023; Liu et al. 2026*a*), spherical particles were adopted in this study as a computationally driven compromise. To obtain representative results for gap-graded soils, each specimen required at least 500 coarse particles, which substantially increased the number of finer particles and contacts, making shearing to the critical state computationally intensive. Incorporating realistic particle shapes would further escalate the computational cost. This simplification enabled the focus to be placed on particle size distribution and stress-transmission efficiency under controlled conditions. This limitation is acknowledged, and future work will incorporate realistic particle shapes when greater computational resources become available. Periodic boundary conditions were applied to minimize boundary influences (e.g., Thornton 2000) without gravitational forces. The Hertz–Mindlin contact model (Shire 2014) was employed, considering three key particle properties: particle Young's modulus (E_{p}), Poisson's ratio (υ_{p}), and the inter-particle friction coefficient (μ). This model has been widely validated in experimental studies and is generally more suitable for simulating granular materials than simpler linear models. However, it is acknowledged that different particle interactions could, in principle, be governed by different contact models. Thus, the use of a uniform Hertz–Mindlin model represents a numerical simplification in this study. The model parameters were carefully selected based on prior experimental findings (e.g., Sandeep and Senetakis 2018; Liu et al. 2026*b*; Nardelli and Coop 2019; Liu et al. 2025), ensuring their appropriateness for capturing the key mechanical behavior of gap-graded soils. Figure 1*a* shows microscale experimental results for particle properties, gathered from previous studies on commonly observed granular materials. These include various quartz sands such as beach sand and river sand (Sandeep et al. 2018), Eglin sand (Nardelli et al. 2017), Fujian sand (Liu et al. 2019*a*; Liu and Lourenço 2021; Liu et al. 2024*a*), and Leighton Buzzard sand (e.g., Senetakis and Sandeep 2017; Nardelli and Coop 2019). Consequently, the selected particle properties fall within these experimental ranges, providing a geologically reasonable basis for the adopted parameters.

As presented in Fig. 1, a correlation was found between the inter-particle friction coefficient during shearing stage (μ_{s}) and the particle Young's modulus (E_{p}), indicating that higher values of μ_{s} correspond to lower E_{p} and vice versa. Three distinct cases were considered in this study:

(1) **Case 1**: Both coarse and finer particles were assigned identical properties with $E_{\mathrm{p}} = 70$ GPa, $\mu_{\mathrm{s}} = 0.25$, and Poisson's ratio (υ_{p}) = 0.2. These values are averages derived from the results presented in Fig. 1*a* and are consistent with those used in prior DEM studies (e.g., Huang 2014).
(2) **Case 2**: The properties of coarse particles remained unchanged, while finer particles were assigned a lower E_{p} of 30 GPa and a higher μ_{s} of 0.45, with υ_{p} remaining at 0.2.
(3) **Case 3**: Coarse particle properties were kept constant, whereas finer particles were given a higher E_{p} of 110 GPa and a lower μ_{s} of 0.15, again with the same υ_{p}. As discussed earlier, the Hertz–Mindlin contact model was employed in the present DEM simulations (eqs. 1–3). The variations in particle Young's modulus (E_{p}) and inter-particle friction coefficient (μ_{s}) have a pronounced influence on the overall soil response. In particular, the contact stiffness, governed by the E_{p} values of both interacting particles, plays a key role in determining the macroscopic mechanical behavior. Although a decoupled parametric analysis of friction coefficient and elastic modulus is important, the present study focuses on the combined effect of particle property disparity in gap-graded soils to elucidate stress transmission mechanisms. The independent roles of these parameters have been systematically examined in previous studies (e.g., Liu et al. 2026*b*).

All particles were randomly distributed in noncontacting positions using a custom placement algorithm. They were subjected to periodic isotropic compression until a target mean effective stress (p') was reached, following the procedure described by Cundall (1988). The formation of

Fig. 1. The discrete element method (DEM) configurations: (*a*) particle property disparity; (*b*) particle size distributions; (*c*) representative DEM specimens.

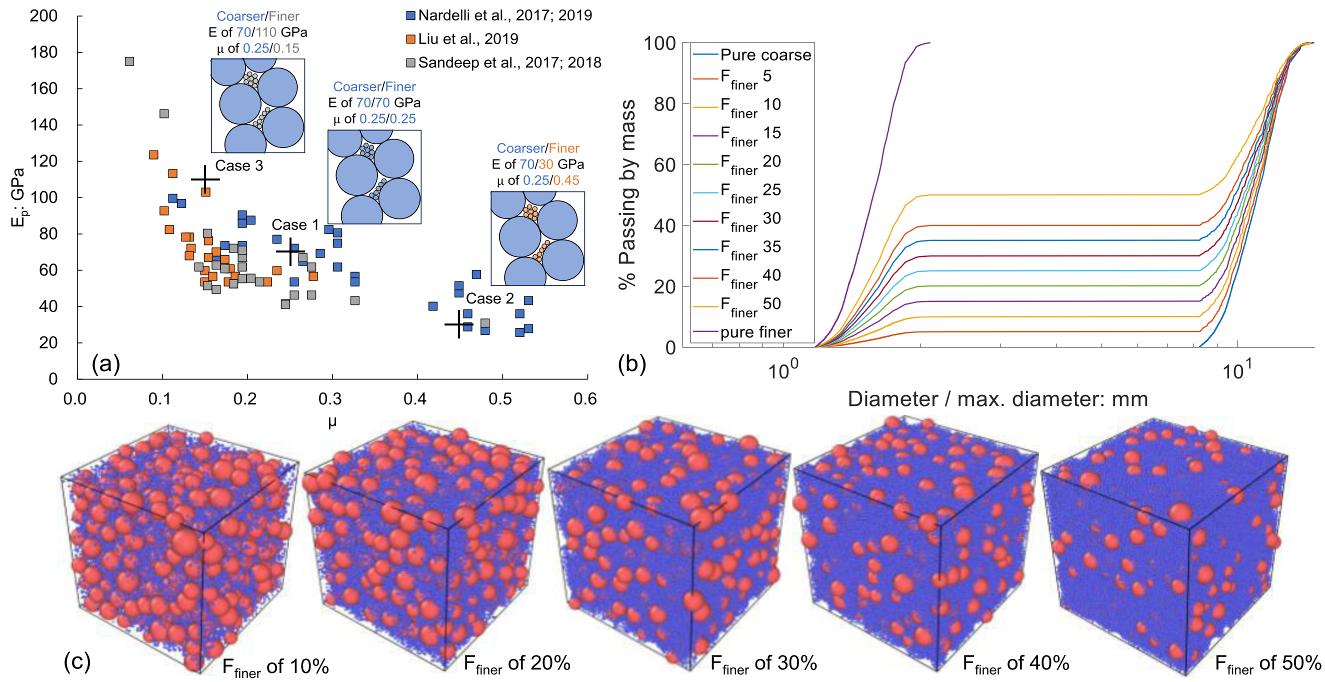

gap-graded soils with varying percentages of finer particles F_{finer}—specifically 5%, 10%, 15%, 20%, 25%, 30%, 35%, 40%, and 50%—is illustrated in Fig. 1*b*. For the coarse fraction, sizes range from approximately 8.25 to 14.60 mm, whereas the finer fraction ranges from approximately 1.18 to 2.09 mm. It is noted that the term "finer particles" in this study does not refer to fine-grained soils (i.e., particles smaller than 0.075 mm) but instead denotes the smaller particle group within a controlled bidisperse granular system (e.g., Thornton 2000; Shire et al. 2016), defined relative to the coarse fraction. Besides, for $F_{\text{finer}} = 5\%$, 10%, 15%, 20%, 25%, 30%, 35%, 40%, 50%, the corresponding C_{υ} values are approximately 1.28, 5.43, 6.65, 6.97, 7.16, 7.26, 7.29, 7.22, and 7.02, respectively, while the corresponding C_c values are approximately 0.99, 4.11, 4.94, 5.08, 4.90, 4.31, 0.21, 0.20, and 0.20. These results indicate that neither C_u nor C_c adequately characterizes the gradation of the present gap-graded soils. This limitation arises because both parameters are defined based on a limited number of characteristic particle diameters and therefore do not capture the full features of noncontinuous gradation curves. In contrast, as demonstrated in Liu et al. (2024*c*), grading indices that incorporate the entire particle size distribution provide a more appropriate description of gap-graded soils, as they account for the contributions of all particle fractions.

Representative specimens for these F_{finer} are presented in Fig. 1*c*. A constant particle size ratio of approximately 7.0 between coarse and finer particles (D_{50}/d_{50}) was employed, where D_{50} and d_{50} denote the median diameters of the coarse and finer particles, respectively. Previous studies (Lade et al. 1998; Shire et al. 2016) have shown that a size ratio of 6.5 is adequate for ensuring that a finer particle can fit within the smallest constriction formed by three coarse particles. Furthermore, when the size ratio exceeds 6.5, the stress transmission characteristics among gap-graded soils remain largely unchanged (e.g., Liu et al. 2023).

Building upon the methodology from Sufian et al. (2021), each specimen contained more than 500 coarse particles to ensure the use of representative elementary volumes for these gap-graded soils. As F_{finer} increases, the total number of particles varies from 10 410 to 178 193. To investigate the state-dependent behavior of granular materials, three $p^{'}$ of 100, 1000, and 3000 kPa were applied. To ensure consistency with previous DEM and experimental investigations on spherical particles (e.g., Chang and Deng 2020), an upper bound of 3 MPa was selected to examine the stress-level dependence of stiffness and state behavior across a reasonably wide range. Although this level is below the pressure threshold at which significant particle breakage is typically observed (≈10 MPa; de Bono and McDowell 2018), minor crushing or contact yielding cannot be completely excluded. Such effects, if present, may slightly influence the absolute stiffness or compressibility but are not expected to alter the overall stress-dependent trends. To examine the density effect, three inter-particle friction coefficients during the isotropic compression stage (μ_i) were utilized: (1) μ_i of 0.001 to generate relatively dense specimens; (2) 0.1 for medium-density specimens; (3) 0.3 for relatively loose specimens, resulting in a total of approximately 200 simulations. This specimen generation approach facilitated the consistent creation of different packing configurations.

 Can. Geotech. J. **63:** 1–20 (2026) | dx.doi.org/10.1139/cgj-2026-0215

Fig. 2. Variation of void ratio with increasing F_{finer}: (*a*) discrete element method study; (*b*) lab study (Zuo and Baudet 2015).

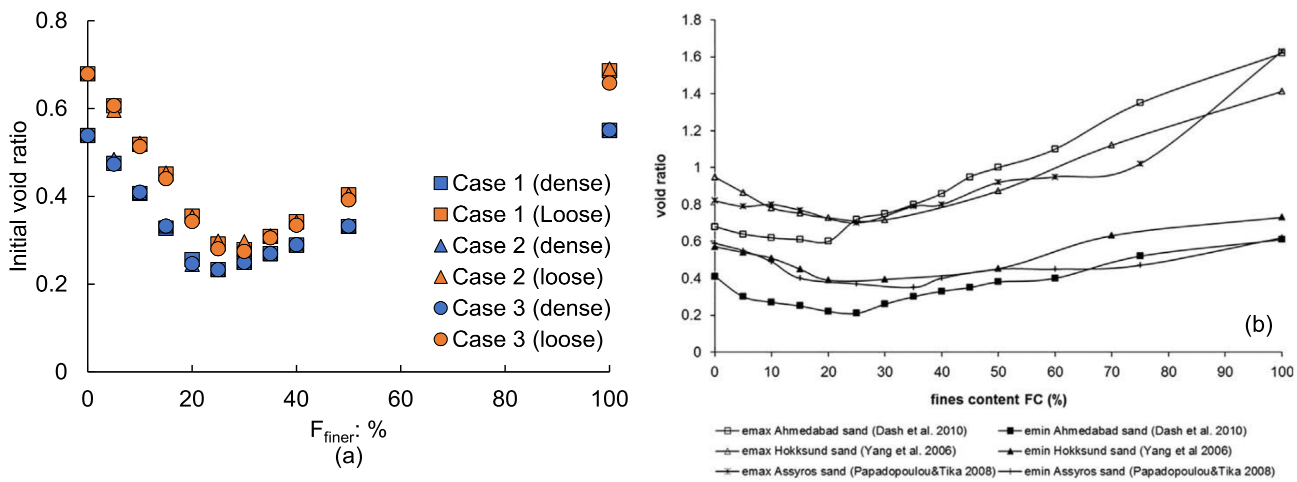

After each specimen achieved its target p' values, the (μ_{i}) values were replaced with the desired μ_{s} values specified before. A relaxation phase was then executed to establish a stable, quasi-static condition, confirmed by ensuring that the coordination number (Z) (the average number of contacts per particle) remained constant, with variations less than 0.001, over approximately 500 000 simulation cycles before ending the compression stage (Liu et al. 2021). Subsequently, triaxial compression simulations were conducted with small increments to study the elastic behavior of the granular materials, followed by drained triaxial shearing until critical states were reached.

3. Results and discussion

Figure 2*a* then illustrates the variations of initial (i.e., at the end of isotropic compression stage) with increasing F_{finer} for these three cases in both dense and loose packing conditions. Both the initial and critical void ratio characteristics exhibit similar trends for all cases, despite the particle property disparity between coarse and finer particles. This is because the finite E_{p} disparity among particles is insufficient to significantly affect overlap behavior in the Hertz–Mindlin contact model, therefore, not strongly affecting void ratio characteristics. Figure 2*a* presents the minimum void ratio values occur at a F_{finer} of 25% for dense specimens and 30% for loose specimens, aligning with observations from prior studies on void ratio characteristics. These results were further validated against previous experimental observations (Fig. 2*b*), such as those reported by Zuo and Baudet (2015), which exhibit a consistent trend of void ratio variation with increasing F_{finer}. Both numerical and experimental data indicate a minimum void ratio at $F_{\text{finer}} \approx 25\%-35\%$, depending on factors such as particle size ratio and initial packing density.

Figure 3 shows the particle scale stress distribution to examine the role of finer particles. Two analytical methods were employed, focusing on both contact interactions and particle classifications. Contact force data were used to compute the internal stress transmission within the specimen. The methodology for this calculation is detailed as follows:

$$\sigma'_{ij} = \frac{1}{v}\sum_{C=1}^{N_{\text{c,V}}}\left(f_i^{\text{c}} l_j^{\text{c}}\right) \tag{4}$$

where V denotes volume of specimens, $N_{\text{c,V}}$ denotes the total number of contacts in the volume, f_i^{c} and l_j^{c} denote the force vector and branch vector, respectively. Therefore, the stress transferred by single contact c can be estimated as follows:

$$\sigma'_{\text{c}} = \frac{f_i^{\text{c}} l_j^{\text{c}}}{V} \tag{5}$$

Therefore, by summing the stresses transmitted through all C–C contacts, the total stress carried by coarse–coarse contacts is obtained. The proportion of stress transferred by C–C contacts (α_{cc}) is then calculated by dividing this value by the total mean effective stress. Similarly, the proportions of stress transferred through C–F contacts (α_{cf}) and F–F contacts (α_{ff}) were obtained in the same manner, with $\alpha_{\text{cc}} + \alpha_{\text{cf}} + \alpha_{\text{ff}} = 1$.

This study also explores the stress distribution between coarse and finer particles, in line with prior research (e.g., Weber 1966; Bagi 1996; Potyondy and Cundall 2004; Cambou et al. 2013; Love 2013). The overall effective stress tensor by aggregating the stress tensors of individual particles is calculated as follows:

$$\sigma'_{ij} = \frac{1}{V}\sum_{m=1}^{N_{\text{t}}}\left(\bar{\sigma}_{ij}^{m} V^{m}\right) \tag{6}$$

σ'_{ij} represents the effective overall stress tensor of the specimen. The total number of stress-transmitting particles is denoted by N_{t}. For an individual particle m, the average stress tensor is $\bar{\sigma}_{ij}^{m}$, and its volume is V^{m}. The contribution of each particle m to the overall effective stress $\left(\alpha_{ij}^{m}\right)$, is calculated as

Fig. 3. Stress transmission at the initial soil state based on (*a*) contact types in the dense conditions; (*b*) particle types in the dense conditions; (*c*) stress transmission efficiency in dense conditions; (*d*) stress transmission efficiency in loose conditions.

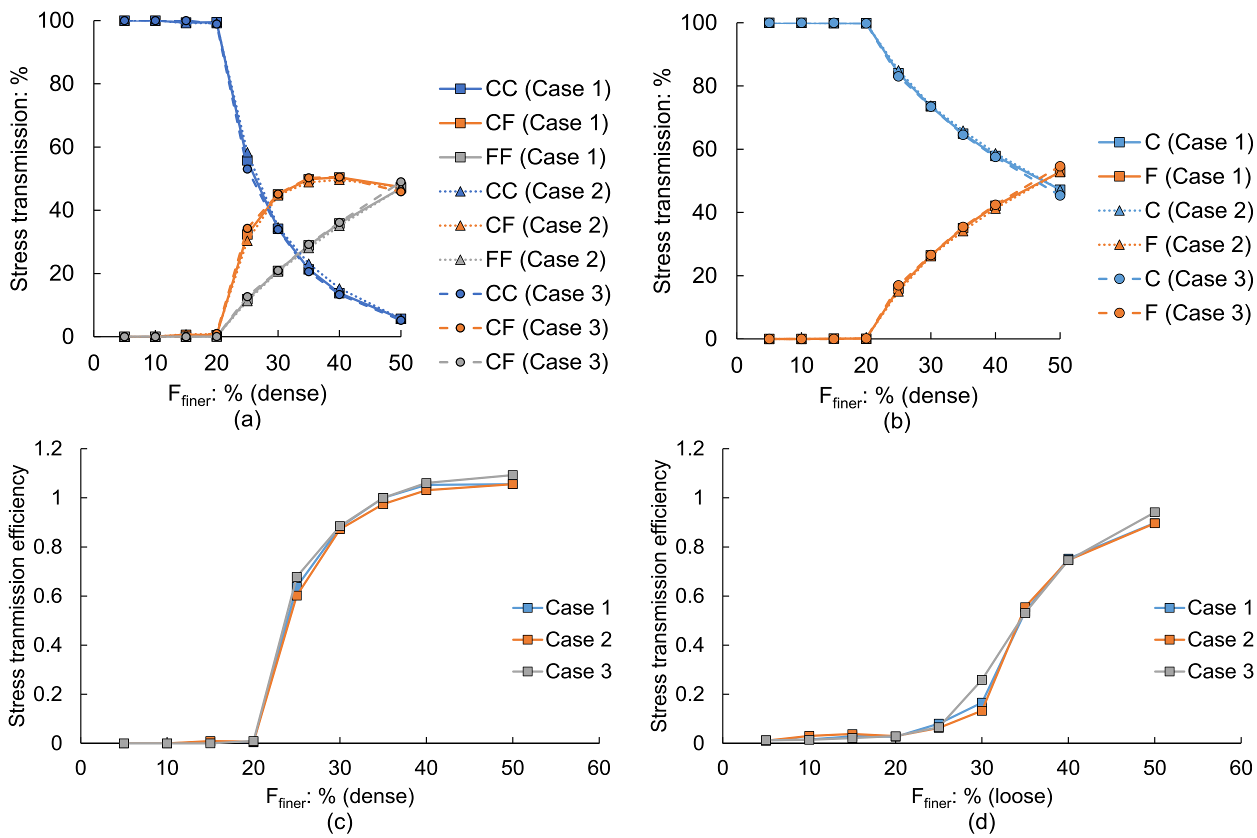

follows:

$$a_{ij}^{m} = \frac{\bar{\sigma}_{ij}^{m} V^{m}}{V} \tag{7}$$

By employing this dual methodology, the stress transmission within gap-graded soil specimens can be clearly distinguished. The total stress carried by coarse particles is obtained by summing the stresses transmitted through all coarse contacts, and the proportion of stress transferred by coarse particles (α_c) is calculated by dividing this value by the total mean effective stress. Similarly, the proportion of stress transferred by finer particles (α_f) is obtained in the same manner, with $\alpha_c + \alpha_f = 1$. Generally, this separation enables a detailed analysis of stress distribution based on both contact types—coarse–coarse (CC), coarse–finer (CF), and finer–finer (FF)—and particle types—coarse (C) and finer particles (F). Consequently, the stress contributions from CC, CF, and FF contacts are denoted as α_{cc}, α_{cf}, and α_{ff}, respectively, satisfying $\alpha_{cc} + \alpha_{cf} + \alpha_{ff} = 1$. Likewise, the corresponding stress fractions carried by the coarse and finer particle groups are represented by α_c and α_f, with $\alpha_c + \alpha_f = 1$.

As presented in Fig. 3, all three cases exhibit similar stress distribution characteristics at the initial soil state. For instance, in dense conditions (p' of 100 kPa), when F_{finer} is below 25%, CC contacts predominantly facilitate stress transmission, while CF and FF contacts make negligible contributions. As F_{finer} increases to approximately 25%–30%, the stress transmission contributions of CF and FF contacts become more pronounced. At $F_{\text{finer}} = 50\%$, both CF and FF contacts become substantial contributors to stress transmission. The present results show similar stress transmission patterns to those reported by Minh et al. (2014) for gap-graded soils, further supporting the validity of the adopted contact analysis approach. Figure 3*b* further illustrates the stress distribution by particle type, confirming that the particle property disparity has a limited effect on stress distribution at the initial soil state. Although not presented, the limited property disparity effect on stress distribution at the initial soil state was also observed in both medium and loose conditions.

To quantify the stress contribution of finer particles, a metric called "stress transmission efficiency" was introduced, defined as the ratio of the proportion of the stress transferred by finer particles to its F_{finer}.

$$\eta_S = \frac{\alpha_f}{F_{\text{finer}}} \tag{8}$$

Note that the α_c and α_f are the proportion of the stress transferred by coarse and finer particles, respectively. The proposal of stress transmission efficiency, η_s, clearly demonstrates an index demonstrating the capability of finer particles for transferring stress. Variations in stress transmission

 Can. Geotech. J. 63: 1–20 (2026) | dx.doi.org/10.1139/cgj-2026-0215

Fig. 4. Variation of stress ratio for representative specimens: (*a*) Case 1 in dense; (*b*) Case 2 in dense; (*c*) Case 3 in dense; (*d*) Case 1 in loose; (*e*) Case 2 in loose; (*f*) Case 3 in loose.

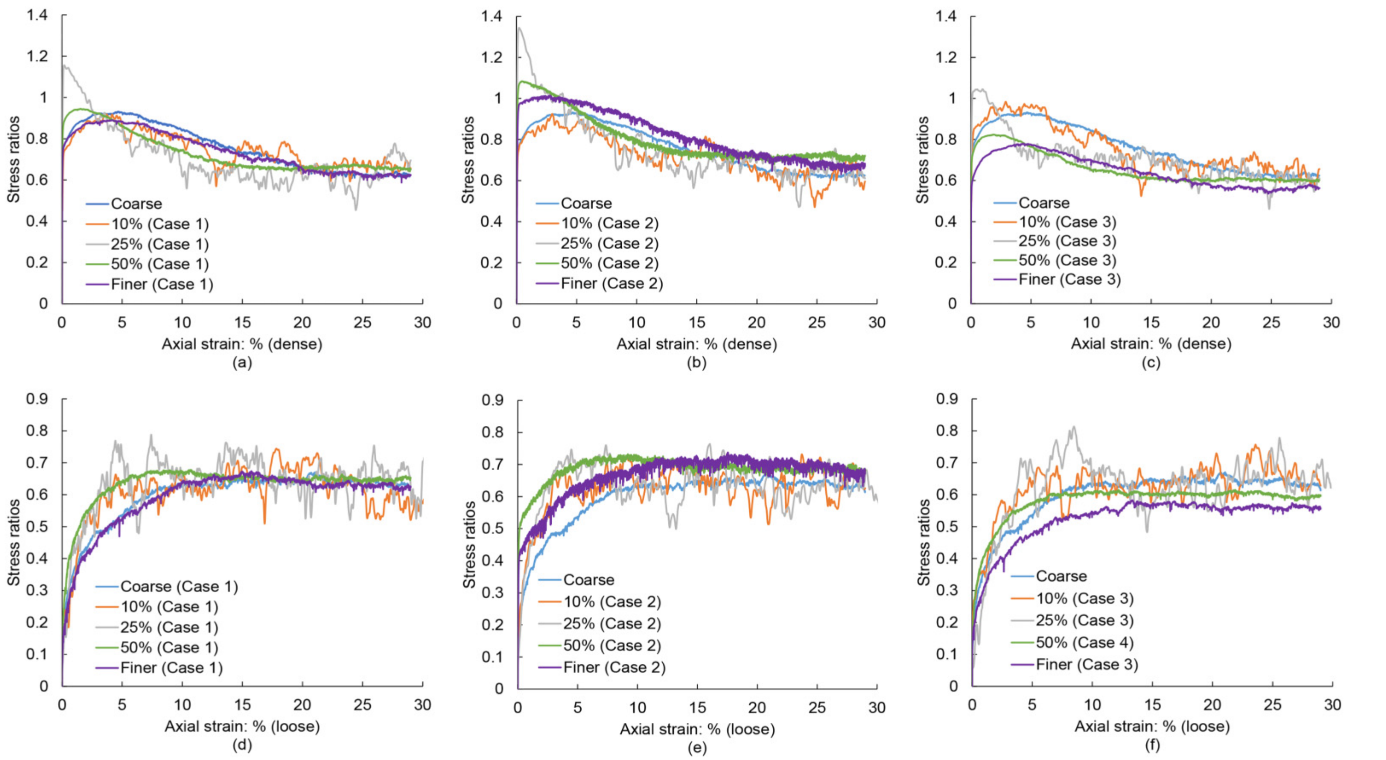

efficiency (η_s) reflect the evolving participation of finer particles in the load-bearing framework and are directly linked to key macroscopic behaviors. Lower α indicates that stress is mainly carried by coarse particles, resulting in higher compressibility, stronger dilatancy, and greater susceptibility to suffusion due to limited interlocking. As η_s increases, finer particles begin to participate in force transmission, reducing compressibility and dilatancy while enhancing structural stability.

Figures 3*c* and 3*d* then illustrate efficiency values under dense and loose conditions, respectively. Particle property disparity between coarse and finer particles does not significantly impact the stress transmission efficiency at the initial state. This may be due to the fact that without shear deformation, the stress distribution is predominantly influenced by the particle packing structure, with individual particle properties playing a secondary role. Moreover, a pronounced density effect is observed when $F_{finer} \leq 25\%$, demonstrating higher efficiency values in dense conditions and lower values in loose conditions. For instance, under dense conditions, the stress transmission efficiency reaches a value of 1.0 only when F_{finer} is 50%, attaining approximately 1.04. Only in these overfilled scenarios are finer and coarse particles equivalent in terms of stress transmission. In contrast, under loose conditions, the stress transmission efficiencies remain below 1.0 even at a high F_{finer} of 50%, suggesting that finer particles are inferior to their coarse counterparts in stress transmission. This underscores the complexity of gap-graded soils, where the efficiency of finer particles varies with their fraction and packing density, complicating structural design.

Figure 4 then presents the shearing behavior of representative specimens with F_{finer} of pure coarse, 10%, 25%, 50%, and pure finer when mean effective stress (p') is 100 kPa. Figures 4*a*–4*c* present the shearing responses for Case 1, Case 2, and Case 3 under dense conditions. Similar shearing behavior is observed for the pure coarse and 10% F_{finer} specimens, where active finer particles are nearly absent. As F_{finer} increases to 25% and 50%, finer particles begin to participate in stress transmission, leading to distinct behaviors among these three cases. Stress ratios vary—relatively high in Case 2, moderate in Case 1, and lower in Case 3. For instance, at a 50% F_{finer} at the dense condition, the peak stress ratios are approximately 0.95, 1.1, and 0.83 for Case 1, Case 2, and Case 3. This pattern agrees with prior studies (Huang 2014), indicating that higher μ_s values lead to increased stress ratio values. Moreover, Figures 4*d*–4*f* present the shearing responses for the same cases under loose conditions, demonstrating the typical loose shearing characteristics for these representative specimens. Notably, all specimens reach a critical state at axial strains exceeding 25%. Generally, the stress–strain trends agree well with those reported by Gong et al. (2019*a*), although the present stress ratios are slightly lower due to the spherical particle assumption.

Figure 5 illustrates the variation of void ratio during shearing stage for the same set of representative specimens, which reflects the volumetric strain of the specimens. Specifically, Figs. 5*a*–5*c* present the shearing responses for Case 1, Case 2,

Fig. 5. Variation of void ratio for representative specimens: (*a*) Case 1 in dense; (*b*) Case 2 in dense; (*c*) Case 3 in dense; (*d*) Case 1 in loose; (*e*) Case 2 in loose; (*f*) Case 3 in loose.

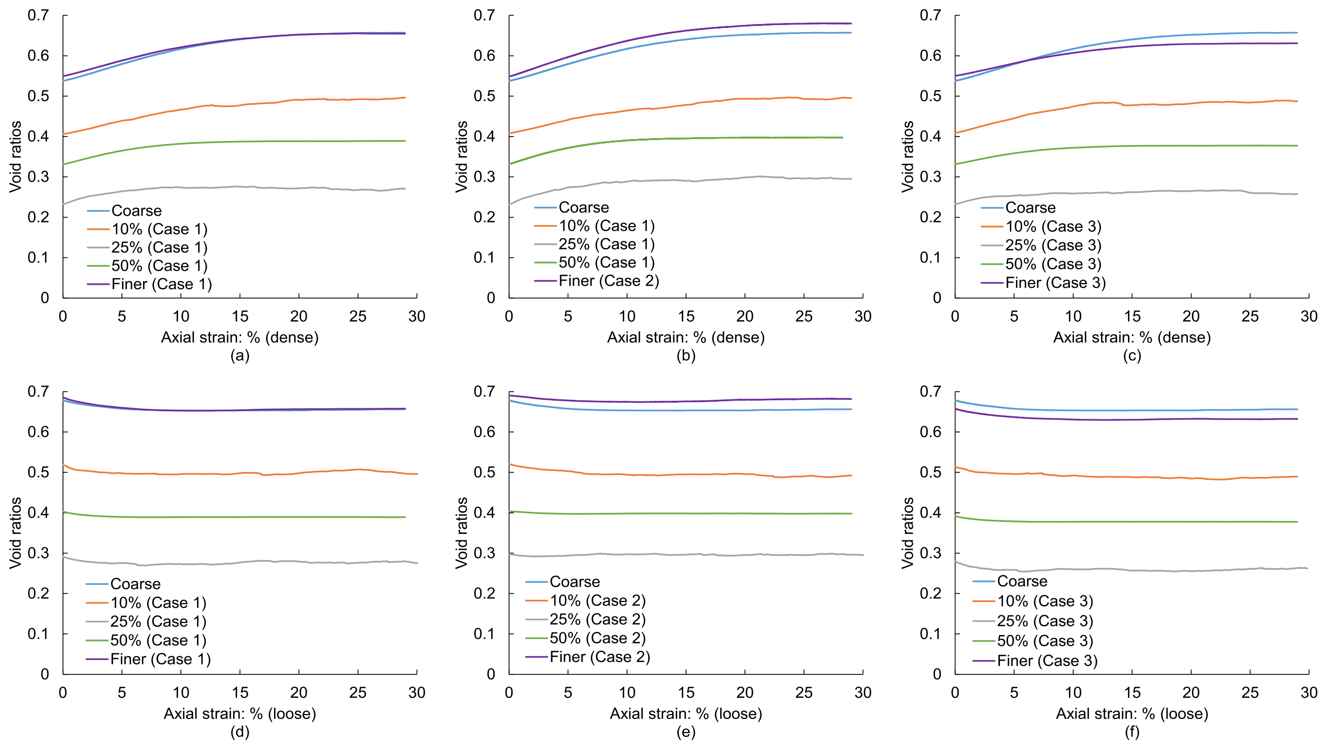

and Case 3 under dense conditions, while Figs. 5*d*–5*f* present the shearing responses for the same cases under loose conditions. Typical dilative behavior is observed in dense conditions, with the void ratio increasing as axial strain increases until the critical state is achieved. Besides, typical contractive behavior can be captured in loose conditions, with void ratio decreasing as axial strain increases, again confirming the attainment of critical states despite the packing density.

Figure 6 illustrates how the coordination number (Z) changes with increasing axial strain for these representative cases with increasing F_{finer} (i.e., 0%, 10%, 25%, 50%, 100%). Note that the coordination number Z is estimated $Z = C_{\text{p}}^{\text{all}}/N$, where C_p^{all} represents the total contact points while N represents the total number of particles (i.e., including all these inactive particles). Besides, there could be two particles contact with each other but do not transfer stress, all these particles were also removed in the calculation process.

Figures 6*a*–6*c* present the evolution of Z with axial strain for these three cases. Compared to Case 1, specimens in Case 2 exhibit lower Z values, while those in Case 3 display higher values. This occurs because higher μ_{s} values among finer particles limit their ability to form contacts, leading to reduced Z values. Additionally, in most instances, the Z values decrease initially but remain stable before the critical state is reached. However, notable exceptions are observed in dense specimens with a F_{finer} of 25%, where the initial Z values are approximately 5.8 and significantly decrease with increasing axial strain. This behavior may indicate a distinctive feature of gap-graded soils, where an overfilled soil structure could transition to an underfilled state, representing a metastable transitional phase. Besides, Fig. 6 reaffirm the density effect, exhibiting negligible Z values when F_{finer} is 25% when referring to loose conditions.

Figure 6*d* provides a deeper quantification of which contact types directly contribute to the decrease in Z values when F_{finer} is 25%. Specifically, the Z values can be divided into three components: $Z\,(\text{CF}) = 2C_{\text{p}}^{\text{cc}}/N$, $Z\,(\text{CF}) = 2C_{\text{p}}^{\text{cf}}$, and $Z\,(\text{FF}) = 2C_{\text{p}}^{\text{FF}}/N$. Here, C_{p}^{CC}, C_{p}^{CF}, and C_p^{FF} represent the total number of CC, CF, and FF contacts, respectively, and N denotes the total number of particles. It is important to note that the overall Z values are the sum of these components: $Z = Z\,(\text{FF}) + Z\,(\text{CF}) + Z\,(\text{FF})$. The analysis reveals that the overall decrease in Z values is directly associated with reductions of Z (CF) and Z (FF). This suggests a significant loss of finer particles as axial strain increases.

Building on the earlier discussion of stress distribution, this study analyzes three representative cases during their shearing stage: (1) $F_{\text{finer}} \leq 20\%$ (underfilled), (2) $25\% \leq F_{\text{finer}} \leq 30\%$ (metastable transitional), and (3) $F_{\text{finer}} \leq 35\%$ (overfilled). In the underfilled case, stress distribution is straightforward, with stress transmission primarily facilitated by CC contacts and coarse particles, due to the negligible presence of active finer particles. This distribution pattern is observed for both mean effective stress $p^{'}$ and deviatoric stress (q) throughout the entire shearing process up to the critical state.

Similarly, following the estimation of α_{cc}, α_{cf}, α_{ff}, α_{c}, and α_{f} at the end of isotropic compression, approximately 1000 strain snapshots were collected during drained triaxial

Fig. 6. Variation of coordination number for representative specimens: (*a*) Case 1; (*b*) Case 2; (*c*) Case 3; (*d*) results of F_{finer} = 25% (D denotes dense; L denotes loose).

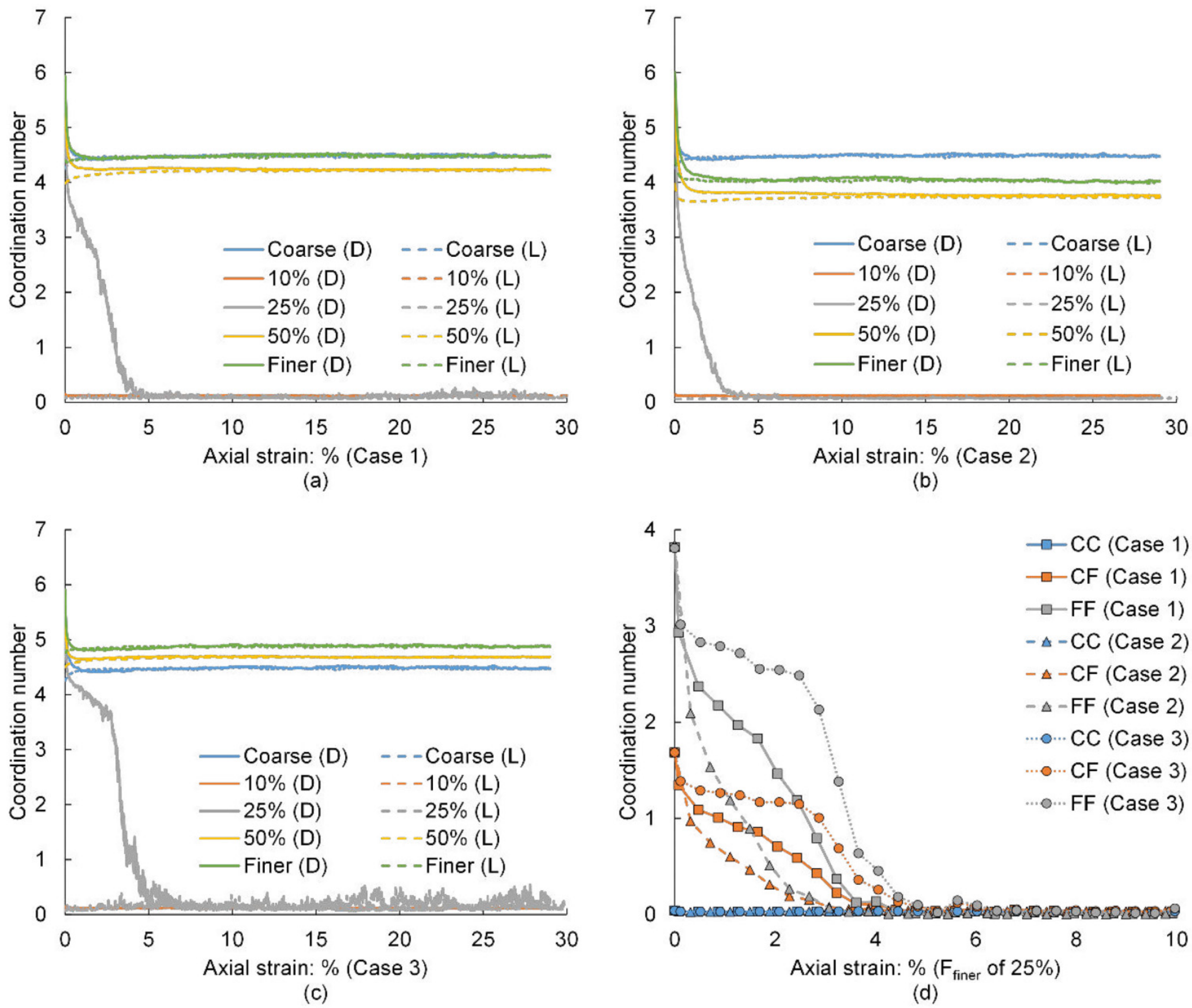

shearing until the critical state was reached. At each snapshot, i, the contact-force-based stress tensor was computed and decomposed by contact type and particle group to evaluate the contributions to the mean effective stress (p'). The corresponding values α^i_{cc}, α^i_{cf}, and α^i_{ff} for C–C, C–F, and F–F contacts, together with α^i_{c} and α^i_{f} for coarse and finer particles, were obtained to describe the evolution of stress distribution of mean effective stress throughout shearing until the critical state.

Figure 7 illustrates the stress distribution of gap-graded soils during shearing when F_{finer} is 25%, representing a metastable transitional case. The stress distribution of p' is presented in Fig. 7*a* from the perspective of contact types under dense conditions. Specifically, Fig. 7*a* reveals that in these three cases, CF and FF contacts begin to participate in stress transmission, especially during the initial stages of shearing. Moreover, the proportion of stress transferred by CC contacts is lowest in Case 2, which is attributed to the relatively lower E_{p} values of finer particles in Case 2. Note that particles with lower E_{p} values tend to carry less load, altering the stress distribution (Liu et al. 2022*b*). However, the proportion of stress carried by CF and FF contacts decreases rapidly with increasing axial strain. This suggests that even under an initially overfilled structure, once shearing is mobilized, the finer-related contacts and finer particles may gradually lose their contribution to maintaining structural stability, leading to their displacement and potentially causing suffusion and similar geotechnical issues. This complexity affects the performance of gap-graded soils in such metastable transitional fabrics, indicating that changes in stress distribution can be observed as axial strain increases up to the critical state.

As discussed earlier, for each individual contact or particle, the local mean effective stress was evaluated as the average of the three principal stress components in the x, y, and z directions, whereas the corresponding deviatoric stress was determined from the difference between the major principal stress (along the z direction) and the mean of the two minor

Fig. 7. Stress distribution during shearing stage when F_{finer} is 25%: (*a*) p' versus axial strain (contact types, dense); (*b*) p' versus axial strain (particle types, Case 1); (*c*) q versus axial strain (contact types, dense); (*d*) q versus axial strain (particle types, Case 1) (D denotes dense; L denotes loose).

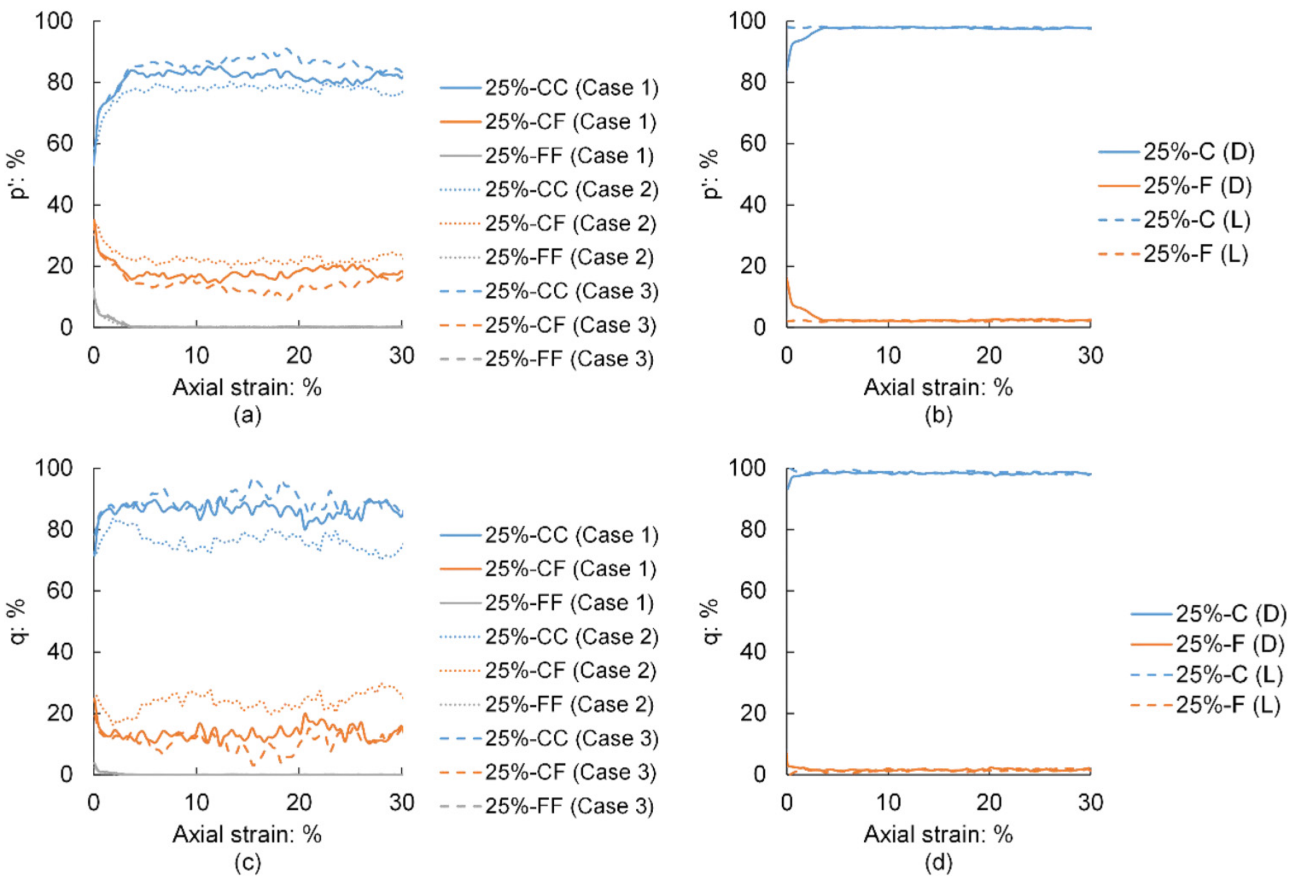

principal stresses (along the *x* and *y* directions). Following this principle, the deviatoric stress distribution (q) can be similarly derived for both contact types and particle types. Specifically, Fig. 7*c* illustrates the stress distribution for q among the three contact types, showing a similar trend to that observed for p'.

Figure 7*b* presents the distribution of p' from the perspective of particle for Case 1, once again highlighting the significant effect of packing density. The results reaffirm the reduction of stress contribution for finer particles with increasing axial strain. Figure 7*d* then demonstrates the q distributions for Case 1, again with density effect being considered. A notable observation is that the proportion of stress carried by finer particles can remain limited even at the onset of shearing, suggesting that their role in transferring q is more restricted compared to their role in transferring p'.

Figure 8 presents the stress distribution characteristics when the F_{finer} reaches 50%. Specifically, Figs. 8*a* and 8*b* present the p' distribution from the perspectives of contact types and particle types, respectively. The effect of particle property disparity is noticeable but limited. Generally, at F_{finer}, CC contacts transfer approximately 7% of the total stress, while CF and FF contacts collectively account for about 46%. The proportions of stress transferred by these contact types remain relatively stable throughout the shearing process, unlike the significant fluctuations observed when the F_{finer} is 25%. Figure 8*b* then illustrates that finer and coarse particles are equivalent in transferring p'.

Figures 8*c* and 8*d* present the stress distribution of q from the perspectives of contact and particle types, respectively. Unlike the pattern observed for p', CC contacts consistently transfer approximately 16% of the deviatoric stress throughout the shearing process, while the proportion carried by FF contacts decreases to about 32% as axial strain increases. This observation further confirms that finer particles have a limited role in transferring q, even at such a high F_{finer}. Figure 8*d* shows that coarse particles contribute significantly more to q—dominating approximately 65%—compared to finer particles, which contribute around 35%. This phenomenon is likely due to deviatoric stress being transmitted through strong force chains, primarily formed by coarse particles with larger size and contact areas. Finer particles, occupying voids, act mainly as fillers, influencing packing density but contributing little to shear resistance.

Figure 9 presents the stress transmission efficiency observed at the critical state, demonstrating the role of finer particles with increasing F_{finer} on both p' and q. Similar results obtained in Figs. 11*a* and 11*b* for the dense and loose

Fig. 8. Stress distribution during shearing stage when F_{finer} is 50%: (*a*) p' versus axial strain (contact types, dense); (*b*) q versus axial strain (contact types, dense); (*c*) p' versus axial strain (particle types, dense); (*d*) q versus axial strain (particle types, dense).

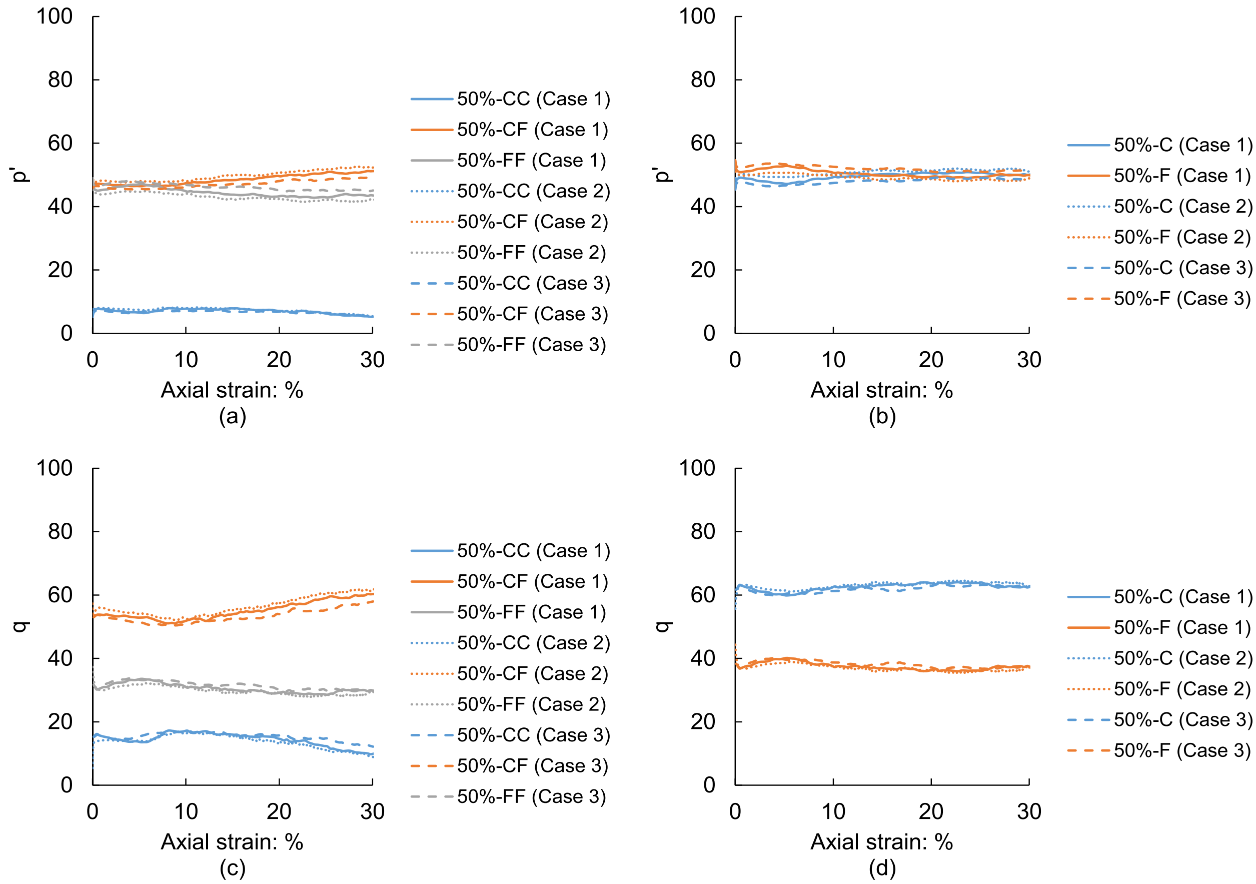

Fig. 9. Stress transmission efficiency at critical state: (*a*) dense condition; (*b*) loose condition.

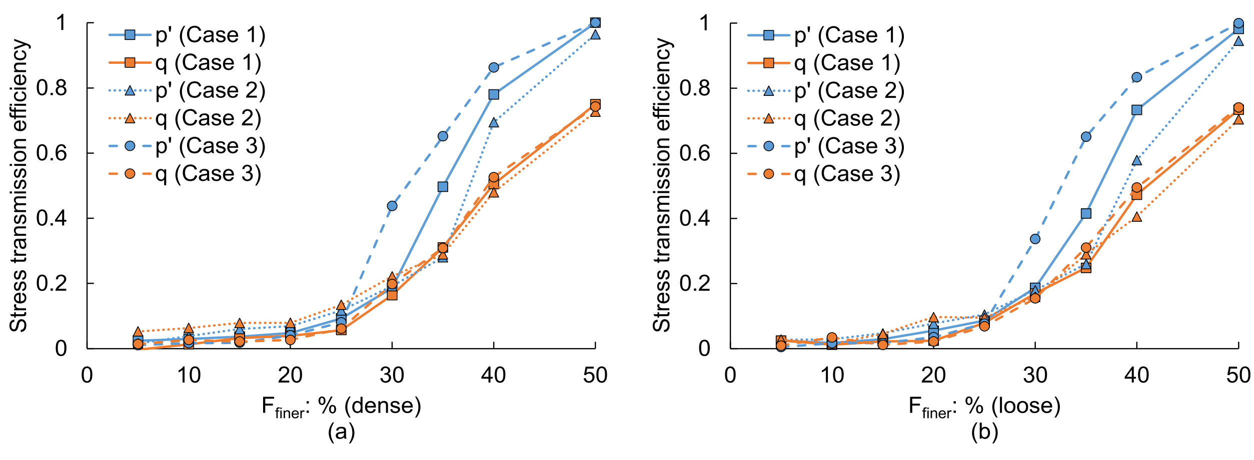

conditions confirm the attainment of the critical state in particle scale. Notably, the stress transmission efficiency of finer particles only reaches 1.0 when the F_{finer} is 50%, and this occurs solely for the p' component. In contrast, for q, the maximum stress transmission efficiency is approximately 0.74. This indicates that coarse and finer particles are not equivalent in transmitting stress, particularly for q. Consequently, it confirms that state variables without accounting for these anisotropic stress distributions may not be fully effective.

Figure 10 presents the critical state lines (CSLs) in q–p' plane of these gap-graded soils. Consequently, Figs. 10*a*–10*c* demonstrate the critical stress ratios for Case 1, Case 2, and Case 3, respectively. Within each case, similar stress ratios

Fig. 10. Critical state lines in $q - p'$ plane for these three cases: (*a*) Case 1; (*b*) Case 2; (*c*) Case 3.

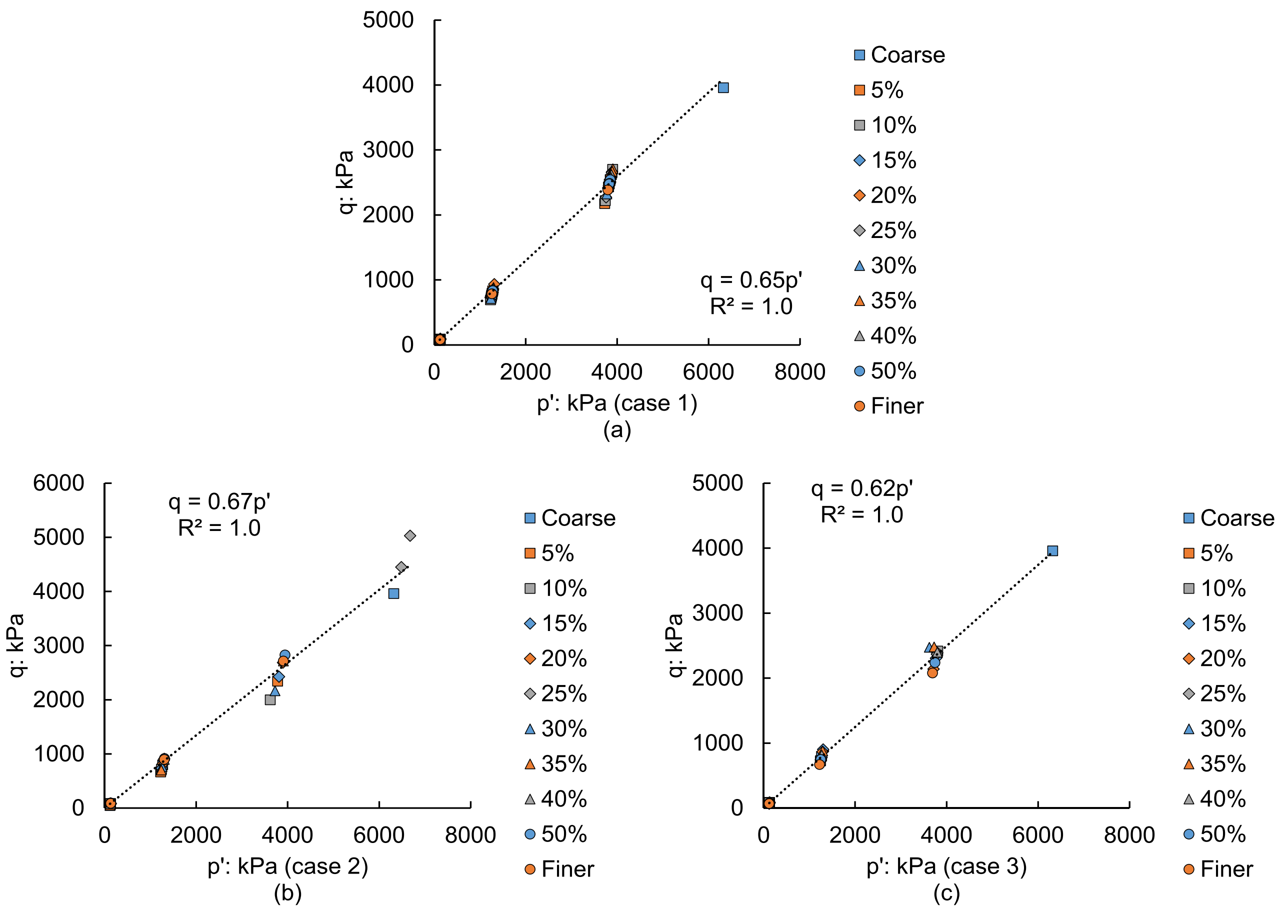

are generally observed with increasing F_{finer}. However, differences can still be observed: higher stress ratios are recorded in Case 2, while lower ones are noted in Case 3. This outcome is expected because finer particles with higher μ_s values in Case 2 actively participate in stress transmission, leading to increased stress ratios. Conversely, in Case 3, the finer particles possess lower μ_s values, resulting in reduced stress ratios.

Figure 11*a* depicts the critical state in the $e - \log p'$ space showing varying F_{finer} leading to different CSLs, which is consistent with observations from previous studies. For these three cases, the CSLs shift downwards as the F_{finer} increases, reaching a minimum when the F_{finer} is approximately 25%. Beyond this point, as the F_{finer} increases from 25% to 50%, the CSLs begin to shift upwards.

Building upon prior research, efforts have been made to establish a unified CSL that encapsulates the behavior of gap-graded soils with increasing F_{finer}. In this study, the mechanical void ratio (e_m), which excludes all inactive particles was employed to model the critical state behavior across varying F_{finer}. As presented in Fig. 12, for F_{finer} ranging from 5% to 25%, a unified fitting curve emerges. This is because most finer particles are inactive in these cases, aligning with the previously proposed concept of the skeleton void ratio (e_s) that neglects finer particles. Moreover, since these three cases share identical coarse particle properties, they exhibit similar CSLs. However, as F_{finer} increases from 30% to 50%, variations in CSLs become evident. This shift is attributed to the fact although finer particles becoming active in stress transmission, their contribution could vary significantly with increasing F_{finer}.

Specifically, Case 1 and Case 3 exhibit similar soil fabric structures at critical states with increasing F_{finer}. These cases show the lowest CSLs when F_{finer} is 30%, with the lines shifting upwards as the F_{finer} increases to 50%. Overall, the CSLs for case 3 are positioned lower than those for Case 1 and Case 2. For instance, at F_{finer} of 50% and p' value of 100 kPa, the critical e_s values are 0.43 for Case 3, 0.46 for Case 1, and 0.51 for Case 2.

A distinct response is observed in Case 2, where finer particles have a higher μ_s. For instance, at $F_{\text{finer}} = 30\%$ and 35%, the critical mechanical void ratios differ markedly under the same mean effective stress but different initial densities, indicating an underfilled fabric in loose and an overfilled fabric in dense conditions. This contradicts the conventional critical state assumption of a unique, density-independent CSL, consistent with prior experimental studies on gap-graded soils (e.g., Shipton and Coop 2015; Xu and Coop 2017). The phenomenon likely arises from the complex role of finer particles, whose contribution to shearing depends strongly on their initial state.

In this study, various proposed state variables were employed to capture the small-strain stiffness characteristics.

Fig. 11. Critical state lines in e−logp' plane: (*a*) Case 1; (*b*) Case 2; (*c*) Case 3.

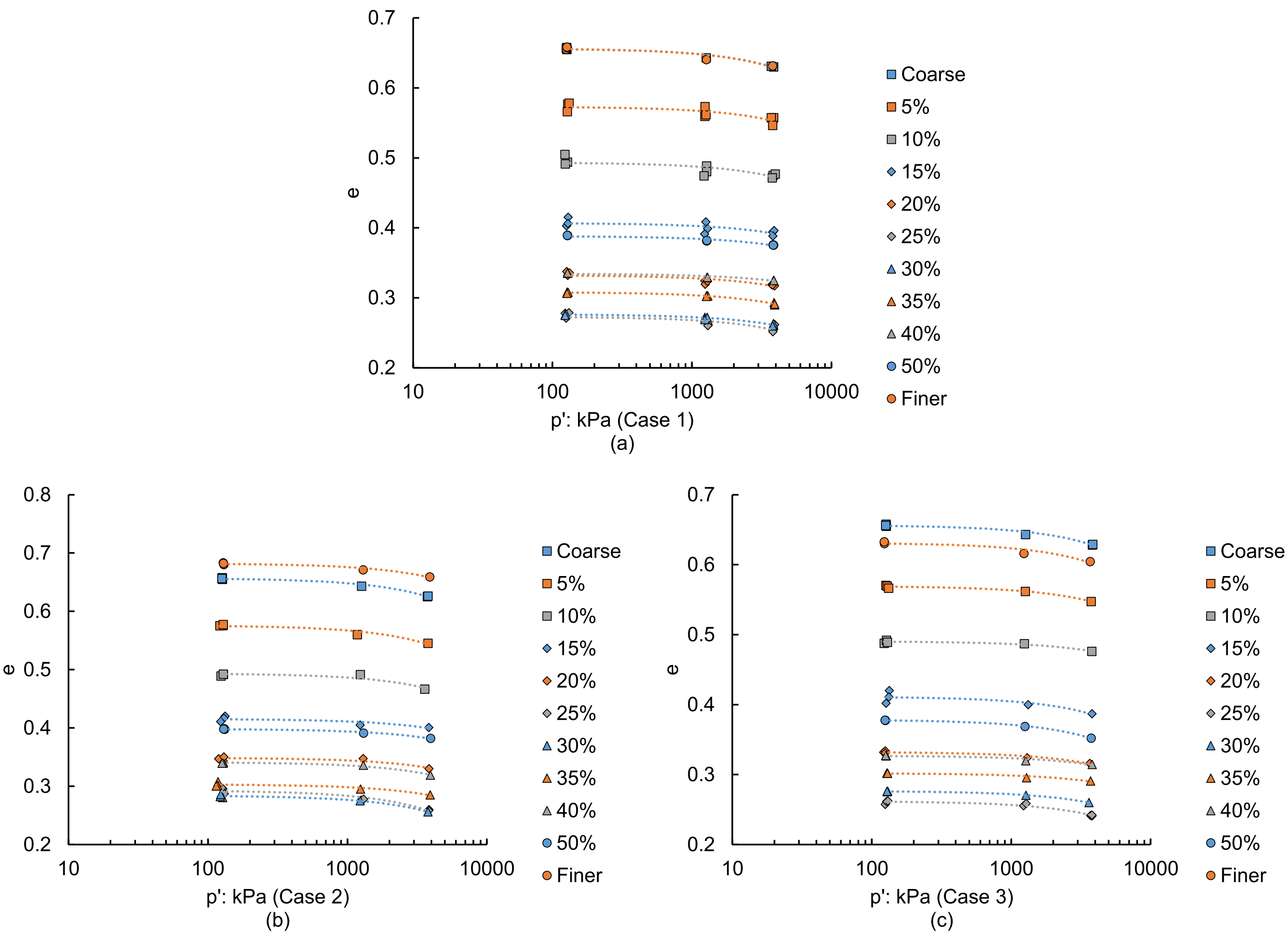

A probe method, which has been used in both experimental and DEM-based investigations was employed to estimate the G_0 values of granular materials (e.g., Kuwano and Jardine 2002; Liu et al. 2024*a*). The G_0 values were calculated using the following equation: $G_0 = \delta q / 3\delta\varepsilon_{\mathrm{p}}^{\mathrm{e}}$, where δq is the increment of deviatoric stress, and $\delta\varepsilon_{\mathrm{q}}^{\mathrm{e}}$ is the increment of elastic deviatoric strain. The elastic deviatoric strain is defined as $\delta\varepsilon_{\mathrm{q}}^{\mathrm{e}} = 2/3\left[\delta\varepsilon_{\mathrm{z}}^{\mathrm{e}} - 0.5\left(\delta\varepsilon_{\mathrm{x}}^{\mathrm{e}} + \delta\varepsilon_{\mathrm{y}}^{\mathrm{e}}\right)\right]$. In this context, $\delta\varepsilon_{\mathrm{z}}^{\mathrm{e}}$ represents the axial elastic strain in the *z*-direction, while $\delta\varepsilon_{\mathrm{z}}^{\mathrm{e}}$ and $\delta\varepsilon_{y}^{e}$ are the elastic strains in the *x*- and *y*-directions, respectively. Following the methodology proposed by Kuwano and Jardine (2002), a deviatoric strain of approximately 10^{-5} is considered appropriate for calculating the G_0.

Figure 13 compares the small-strain stiffness G_0 obtained from DEM simulations with laboratory data for mixtures of identical particle size ratio, ranging from pure coarse to 50% finer fraction. Overall, the simulated G_0−e relationships closely follow the experimental trends, confirming that the DEM captures the essential dependence of stiffness on void ratio and finer fraction. Minor underestimation of G_0 in the DEM results is expected, as the numerical model employs idealized spherical particles and a simplified contact law. Despite these simplifications, the consistent trend across gradations validates the capability of the adopted DEM framework to reproduce the small-strain stiffness behavior of gap-graded soils.

Figure 14 presents the effectiveness of skeleton void ratio (e_{s}) and mechanical void ratio (e_{m}) in capturing small-strain stiffness characteristics of gap-graded soils. For all three cases examined, e_{s} yields satisfactory results when F_{finer} ranges between 0% and 25%. This performance is attributed to the substantial proportion of inactive finer particles present in these cases. Prior criticisms (e.g., Yang et al. 2015) on the use of e_{s} are likely because their size ratio between coarse and finer particles is approximately 4.0, causing finer particles to actively contribute to stress transmission even at low F_{finer}. Additionally, e_{m} shows a trend toward describing the small-strain stiffness characteristics of gap-graded soils in a unified manner as F_{finer} increases. However, scatters are observed in the data, which may be due to the inability of e_{m} to account for the unequal contributions of coarse and finer particles in stress transmission.

Figure 15 illustrates the effectiveness of state parameters in capturing small-strain stiffness in gap-graded soils. Prior studies (e.g., Yang and Liu 2016) have highlighted the superiority of state parameters over e and e_{s} in quantifying small-strain behavior. The state parameter, introduced by Been and

Fig. 12. Critical state lines in $e_{\mathrm{m}}-\log p'$ plane: (*a*) Case 1; (*b*) Case 2; (*c*) Case 3.

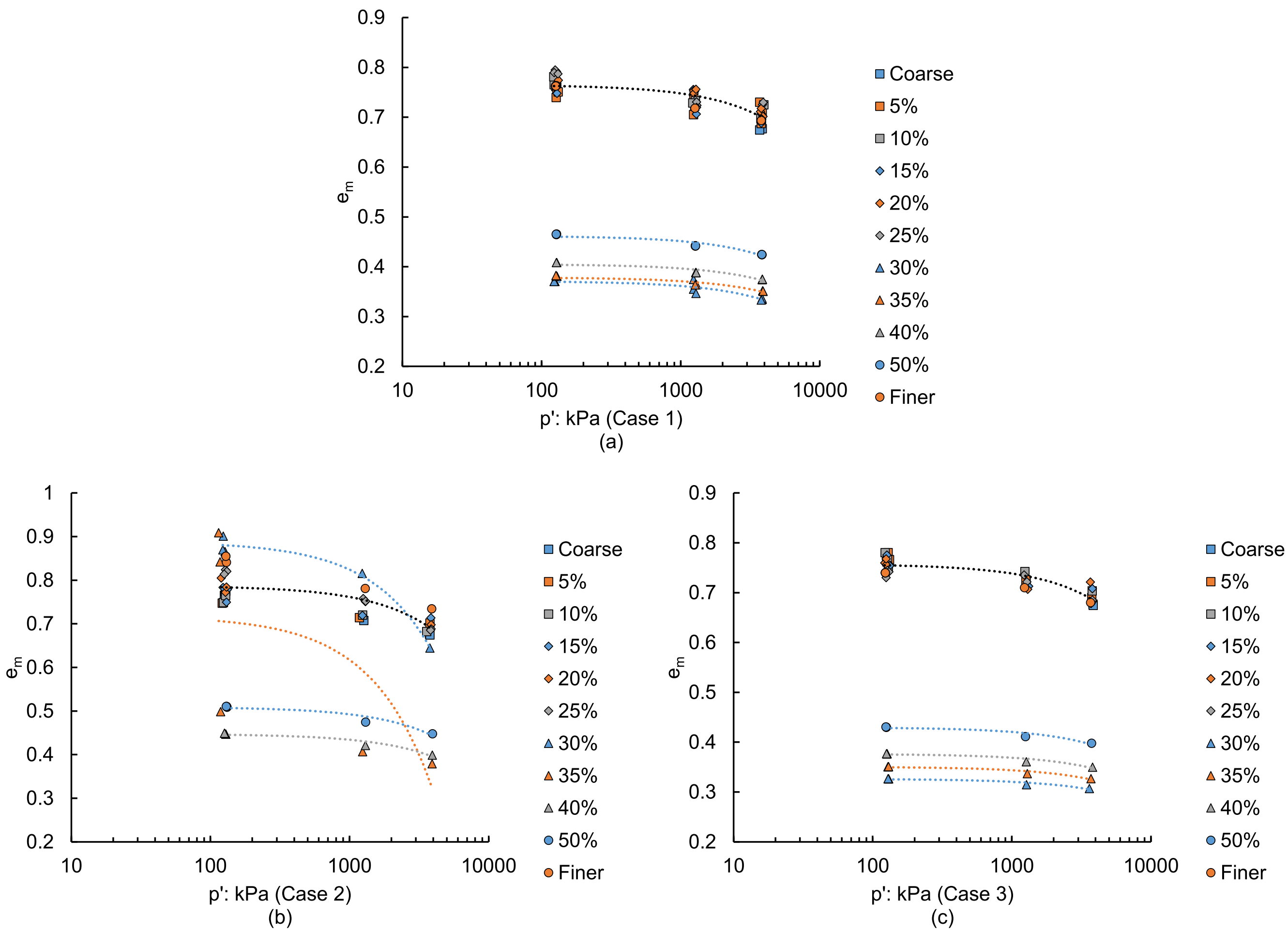

Jefferies (1985), effectively describes the shearing behavior of granular materials, based on initial and critical soil states.

The state parameter (ψ) was employed to quantify the relative density state of the mixtures with respect to their corresponding CSLs, following the concept originally proposed by Been and Jefferies (1985). It is defined as

$$\psi = e - e_{\mathrm{cs}}\left(p'\right) \tag{9}$$

where e is the current void ratio and $e_{\mathrm{cs}}\left(p'\right) = \Gamma - \lambda \ln p'$ represents the void ratio on the CSL at the same mean effective stress p'. The parameters Γ and λ were obtained by fitting the DEM-derived critical state data in the $e-\ln p'$ plane, as shown in Fig. 11. The mean effective stress and void ratio at different loading stages were directly extracted from the simulation results. This definition allows for consistent comparison of the material state evolution across different gradations and densities. However, some recent studies (e.g., Yang et al. 2018) questioned the use of critical state-derived parameters for small-strain elastic behavior, particularly in gap-graded soils. Figure 15 therefore demonstrates the performance of state parameters, which effectively describes small-strain stiffness when F_{finer} is between 0% and 20%, consistent with Yang and Liu (2016). However, significant scatter occurs between 25% and 50%, indicating reduced effectiveness across the full F_{finer} range. Note that the estimation of state parameter were retained without explicitly removing inactive particles, in line with previous experimental studies where inactive particles cannot be identified or excluded. The variability observed in this F_{finer} range suggests that state parameters may not fully account for the different contributions of coarse and finer particles.

This indicates that state parameters do not demonstrate superior performance compared to e_{s} when $F_{\mathrm{finer}} \leq 20\%$. Quantifying state parameters requires accurate CSLs, which are challenging to establish in both experimental and numerical studies. Across a wide F_{finer} range (5%–50%), state parameters fail to describe small-strain stiffness consistently. Nevertheless, they show potential for capturing small-strain behavior when F_{finer} is between 25% and 50%, despite particle property disparity between coarse and finer particles.

Consequently, following Thevanayagam (2000), a refined void ratio was proposed by adjusting the effective volume of finer particles to reflect their partial contribution to the specimens:

$$e' = \frac{\left(v_{\mathrm{t}} - \left(v_{\mathrm{c}} + \alpha v_{\mathrm{f}}\right)\right)}{\left(v_{\mathrm{c}} + \alpha v_{\mathrm{f}}\right)} \tag{10}$$

Fig. 13. Comparison between discrete element method (DEM) simulations and experimental observations of gap-graded soils (e.g., Deyun et al. 2022; Liu 2022): (*a*) pure coarse; (*b*) pure finer; (*c*) F_{finer} of 10%; (*d*) F_{finer} of 25%; (*e*) F_{finer} of 50%.

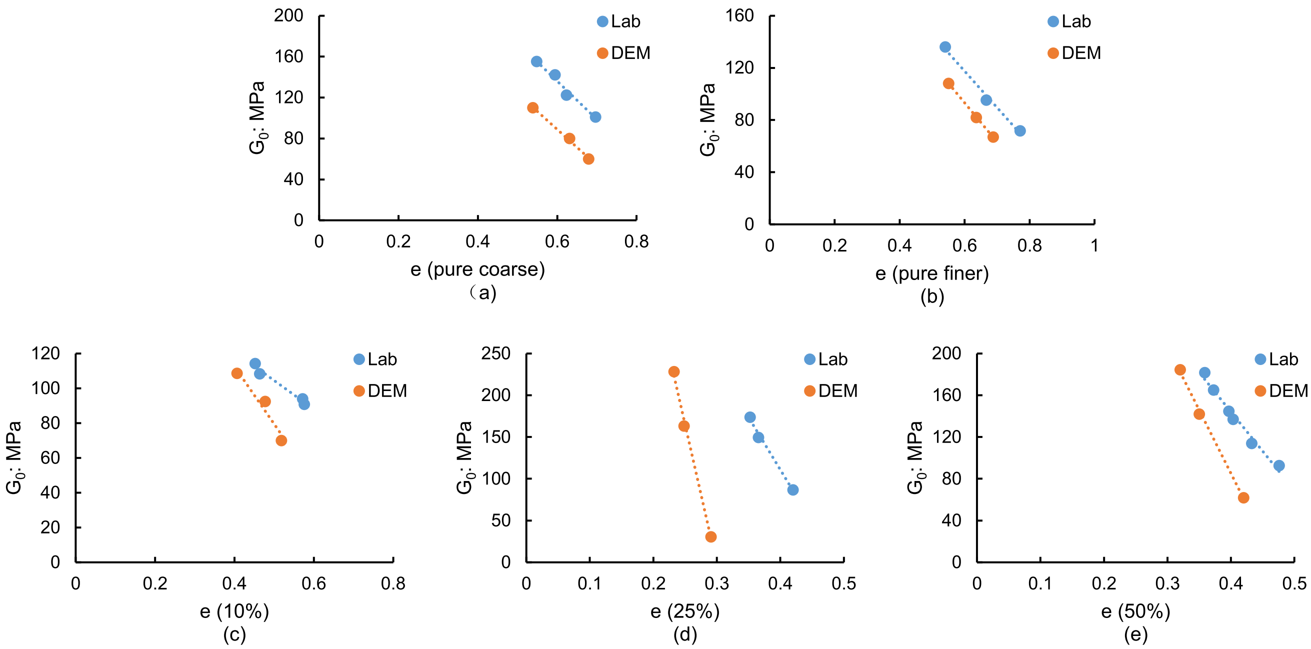

Fig. 14. Performance of e_s and e_m for capturing the small-strain stiffness characteristics: (*a*) Case 1; (*b*) Case 2; (*c*) Case 3.

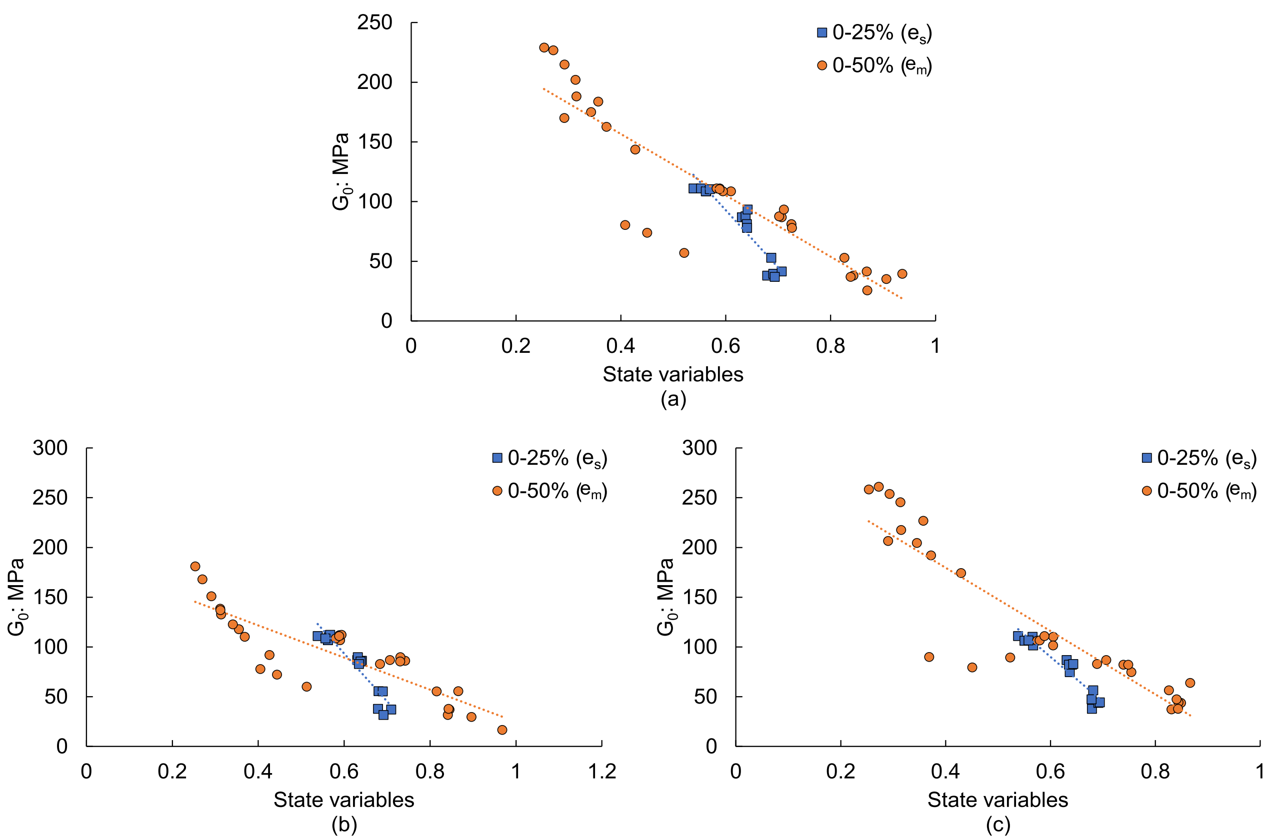

where v_t is the total volume, with v_c and v_f representing the active volumes of coarse and finer particles, respectively. The factor α, used to adjust the effective volume of finer particles, is estimated as $\eta_s \eta_p$, where η_s is the stress transmission efficiency of finer particles (Fig. 3*c*), and η_p accounts for particle property disparities between coarse and finer par-

Fig. 15. Performance of state parameters for capturing the small-strain stiffness characteristics: (*a*) Case 1; (*b*) Case 2; (*c*) Case 3.

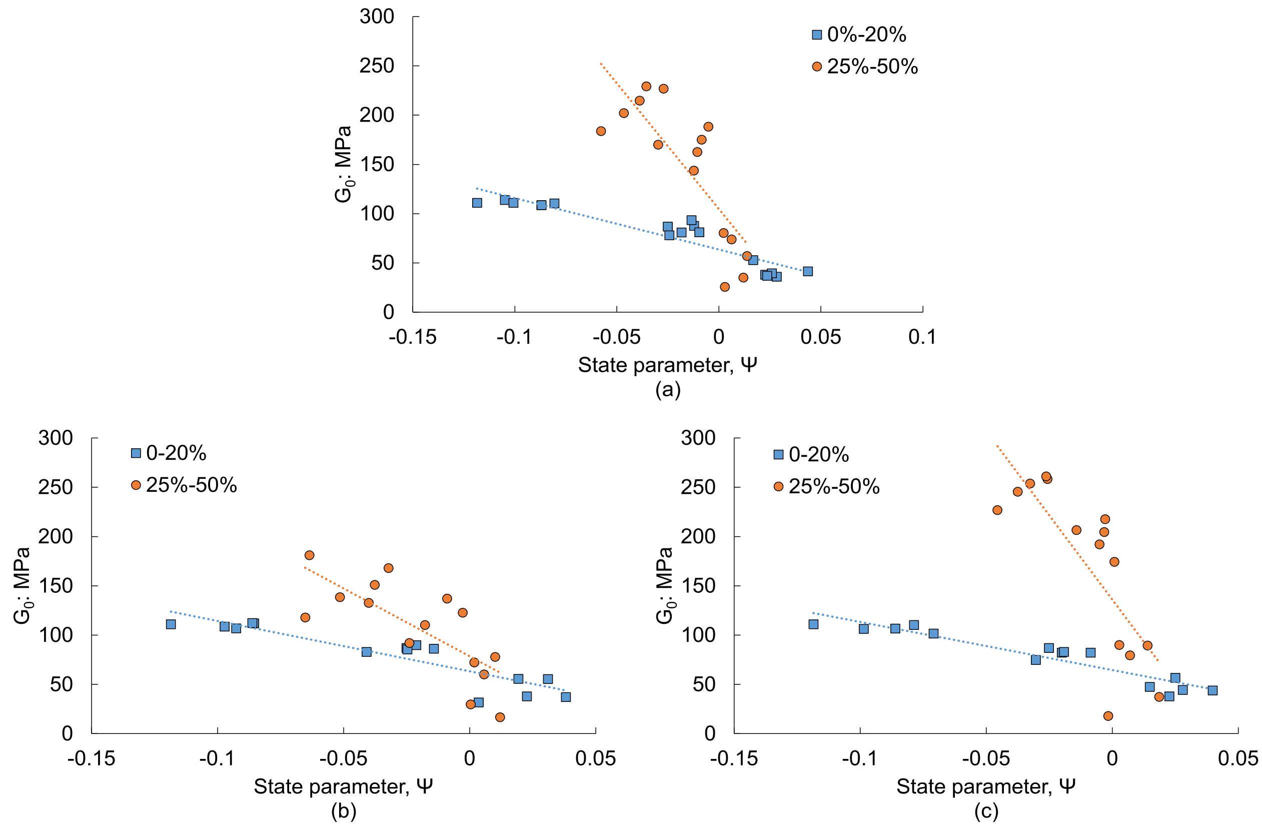

ticles, determined through nonlinear least squares fitting. For Case 1, Case 2, and Case 3, η_p values of 1.0, 0.7, and 1.15, respectively, were obtained, exhibiting improved accuracy in capturing small-strain stiffness as F_{finer} increases. This is demonstrated in Figs. 16*a*–16*c* for Case 1, Case 2, and Case 3, respectively. These η_p values align with the initial configurations of the three cases, demonstrating lower contribution effects in Case 2 due to lower E_p values and higher contribution efficiency in Case 3 due to higher E_p values. The results validate the importance of accounting for the nonequivalent roles of coarse and finer particles when developing state variables.

Figure 17 presents the application of the same methodology to derive the refined void ratio for characterizing the critical state behavior of gap-graded soils. The refined void ratios are calculated by adjusting the effective volume of finer particles, using η_s values determined at the critical state for deviatoric stress and η_p values obtained through nonlinear least squares fitting, with values of 1.0, 1.05, and 0.94 for Case 1, Case 2, and Case 3, respectively. Figure 17 demonstrates that this method again effectively captures the critical state behavior across a wide F_{finer} range (0%–100%). Despite some scatters, a unified curve fitting emerges as F_{finer} increases, supporting the assumption that the nonequivalent roles of active coarse and finer particles should be accounted for in soil behavior modeling. It should be noted that these η_p values were obtained at the critical state and differ from their corresponding values obtained at small-strain state. This suggests that strain state is also an influential factor when studying gap-graded soils.

The refined void ratio effectively captures the evolving role of finer particles in the load-bearing skeleton of gap-graded soils. Unlike classical formulations, it reflects the nonmonotonic influence of finer fraction on stiffness and critical state soils behavior, revealing the intrinsic complexity of dual-structure mixtures. This measure thus provides a unified and physically meaningful descriptor linking small-strain and critical state behaviors, extending the state-parameter frameworks of sands (e.g., Yang et al. 2018) to gap-graded systems where finer particles become structurally active. While these refined state variables may primarily be obtained through numerical simulations, the findings help explain the varied and sometimes conflicting perspectives in studying gap-graded soils. This variability arises because the behavior of gap-graded soils is highly dependent on the role of finer particles, which dynamically evolves with density, F_{finer}, and strain state (e.g., small-strain vs. critical state). Besides, this study offers practical insights for understanding the behavior of gap-graded soils in engineering applications. For instance, the measured void ratio of silty sand or gap-graded soils can be adjusted using a modification factor, β, to better reflect actual soil conditions. The β values can be informed by simulation results that quantify the role of finer particles under varying finer fractions, densities, and strain levels. In practice, the finer fraction, density, and target strain level of soil samples can be obtained through experimental tests, and

Fig. 16. Performance of refined void ratio for capturing the small-strain stiffness characteristics: (*a*) Case 1; (*b*) Case 2; (*c*) Case 3.

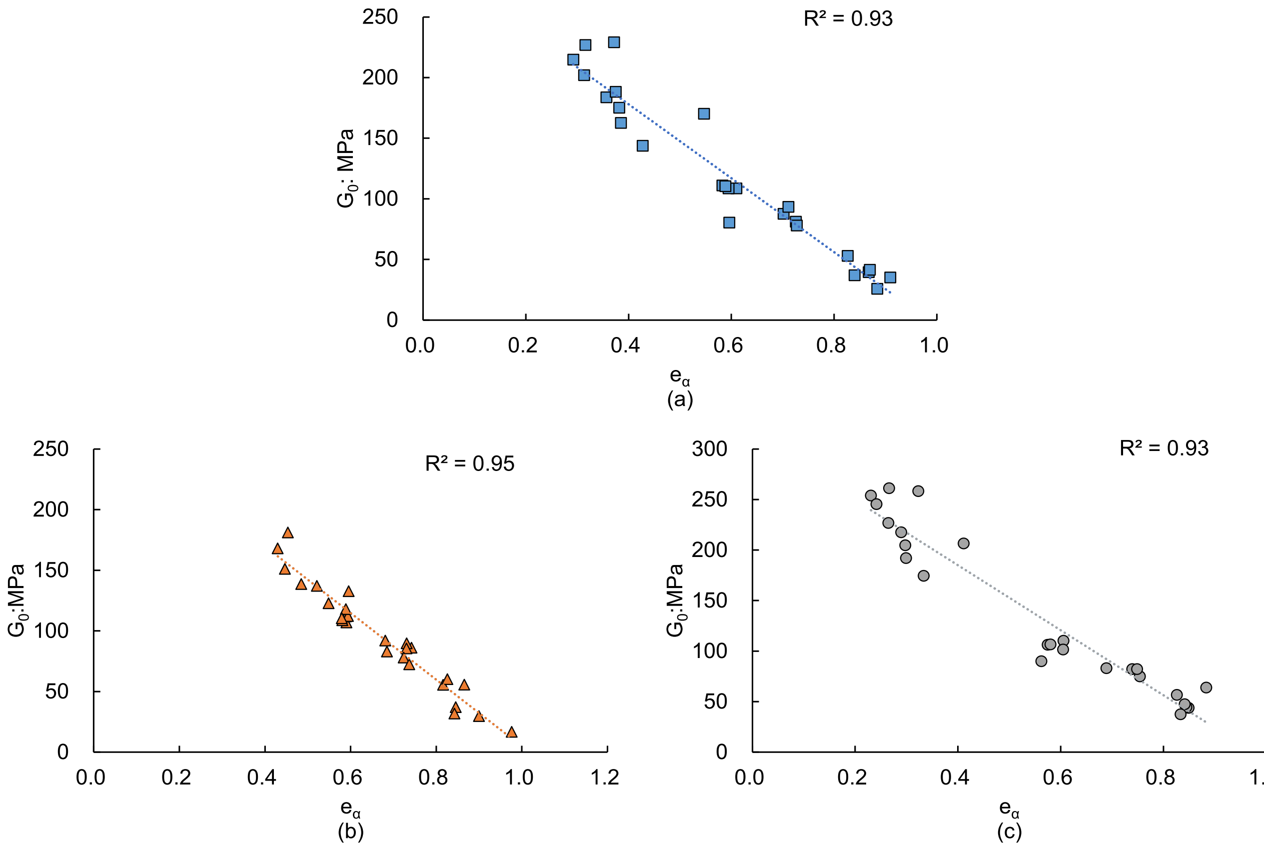

corresponding β values can be referenced from numerical studies. Consequently, comprehensive numerical simulations and validation are desired, considering F_{finer}, density levels, strain level while accounting for realistic particle characteristics, such as particle shape. Due to the high computational demands, this rigorous approach may be explored in future studies.

4. Conclusion

This study employed the DEM to investigate the mechanical behavior of gap-graded soils from small to large strains, explicitly accounting for the disparity in mechanical properties between coarse and finer particles. The main findings are summarized as follows:

(1) The contribution of finer particles to stress transfer strongly depends on finer fraction, density, particle property disparity, and strain level. Finer particles primarily contribute to mean effective stress rather than deviatoric stress, and their effectiveness increases with finer fraction and density. However, finer particles generally remain less efficient than coarse particles in stress transmission. In the metastable transitional regime (e.g., $F_{\text{finer}} \approx 25\%$), their contribution decreases markedly during shearing, indicating reduced capability to sustain soil structure under deformation.

(2) Traditional state variables—such as void ratio, skeleton void ratio, mechanical void ratio, and the state parameter—are inadequate for representing the nonequivalent mechanical roles of coarse and finer particles. These parameters fail to capture the evolving contribution of finer particles across varying densities, strain levels, and particle properties variability, leading to limited accuracy in describing both small-strain stiffness and critical state behavior of gap-graded soils.

(3) A refined state variable was proposed to explicitly incorporate the partial stress contributions of finer particles. This variable successfully captures both small-strain stiffness and critical state characteristics for mixtures with finer fractions up to 100%. By linking these behaviors within a unified framework, it improves the quantitative prediction of mechanical responses across densities and gradations and helps reconcile previously inconsistent interpretations of gap-graded soil behavior.

Additionally, the findings suggest that simulation-informed correction factors may be employed to adjust void ratios for practical applications, enhancing the predictive capability of soil models under varying gradations and

Fig. 17. Performance of refined void ratios for capturing the critical state soil behavior: (*a*) Case 1; (*b*) Case 2; (*c*) Case 3.

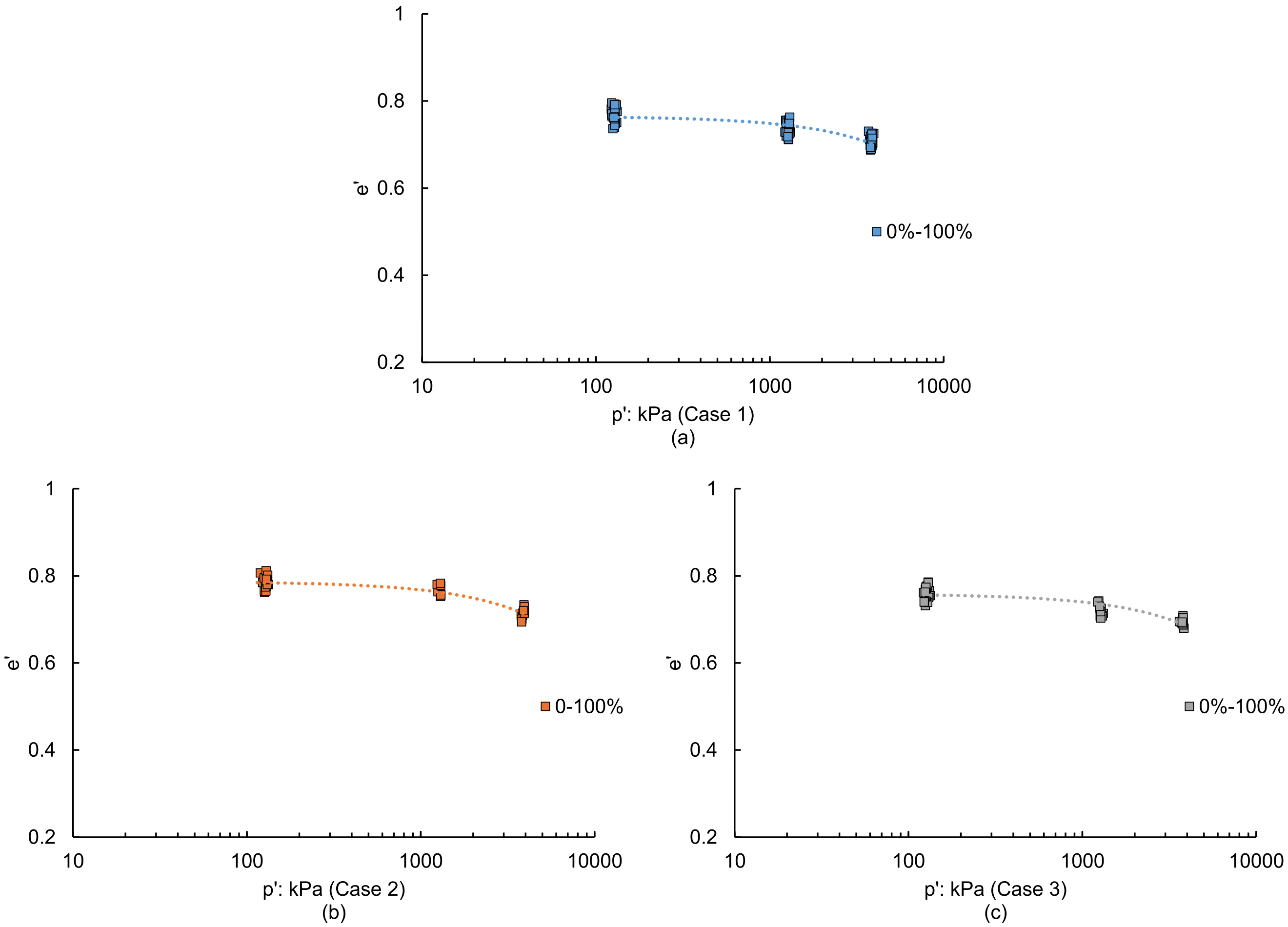

densities. While these results were obtained using spherical particles, extending the conclusions to angular or nonspherical grains should be treated with caution. Nonetheless, the present framework provides a sound basis for future studies incorporating realistic particle geometries and broader stress ranges.

Acknowledgements

This work was financially supported by the Research Grants Council of Hong Kong (GRF No. 16208721; CRF No. C7082-22G; TRS Nos. T22-607/24-N and T22-606/23-R), the National Natural Science Foundation of China (Grant No. 52439001), and the Beijing–Tianjin–Hebei Major Special Project (Grant No. 2025ZD1202700).

Article information

History dates

Received: 10 March 2026
Accepted: 19 May 2026
Version of record online: 24 August 2026

Copyright

Data availability

The datasets generated during and/or analyzed during the current study are available from the corresponding author on reasonable request.

Author information

Author ORCIDs

Shijin Feng https://orcid.org/0000-0002-2811-8006

Author contributions

Conceptualization: DL, SF
Funding acquisition: DL
Investigation: DL, DY
Methodology: DL, DY
Resources: DL, JZ
Software: DL
Supervision: JZ, SF
Visualization: SF

Writing – original draft: DL, DY
Writing – review & editing: DL, SF

Competing interests

The authors have no conflicts of interest to declare that are relevant to the content of this article.

References

Adesina, P., Wautier, A., and Benahmed, N. 2024. A micromechanics-based classification of the regimes delineating the behaviour of gap-graded soils. Computers and Geotechnics, **168**: 106165. doi:10.1016/j.compgeo.2024.106165.

Ahmadi, M., Shire, T., Mehdizadeh, A., and Disfani, M. 2020. DEM modelling to assess internal stability of gap-graded assemblies of spherical particles under various relative densities, fine contents and gap ratios. Computers and Geotechnics, **126**: 103710. doi:10.1016/j.compgeo.2020.103710.

Allen, J.R.L. 1965. A review of the origin and characteristics of recent alluvial sediments. Sedimentology, **5**(2): 89–191. doi:10.1111/j.1365-3091.1965.tb01561.x.

Bagi, K. 1996. Stress and strain in granular assemblies. Mechanics of Materials, **22**(3): 165–177. doi:10.1016/0167-6636(95)00044-5.

Been, K., and Jefferies, M.G. 1985. A state parameter for sands. Géotechnique, **35**(2): 99–112.

Cambou, B., Jean, M., and Radjaï, F. 2013. Micromechanics of granular materials. John Wiley & Sons.

Carraro, J.A.H., Prezzi, M., and Salgado, R. 2009. Shear strength and stiffness of sands containing plastic or nonplastic fines. Journal of Geotechnical and Geoenvironmental Engineering, **135**(9): 1167–1178. doi:10.1061/(ASCE)1090-0241(2009)135:9(1167).

Carrera, A., Coop, M., and Lancellotta, R. 2011. Influence of grading on the mechanical behaviour of Stava tailings. Géotechnique, **61**(11): 935–946.

Chang, C.S., and Deng, Y. 2020. Modeling for critical state line of granular soil with evolution of grain size distribution due to particle breakage. Geoscience Frontiers, **11**(2): 473–486. doi:10.1016/j.gsf.2019.06.008.

Chang, C.S., and Yin, Z.Y. 2011. Micromechanical modeling for behavior of silty sand with influence of fine content. International Journal of Solids and Structures, **48**(19): 2655–2667. doi:10.1016/j.ijsolstr.2011.05.014.

Chang, W.-J., Chang, C.-W., and Zeng, J.-K. 2014. Liquefaction characteristics of gap-graded gravelly soils in K0 condition. Soil Dynamics and Earthquake Engineering, **56**: 74–85. doi:10.1016/j.soildyn.2013.10.005.

Chitravel, S., Otsubo, M., and Kuwano, R. 2023. Effects of seepage flow on liquefaction resistance of uniform sand and gap-graded soil under undrained cyclic torsional shear. Soils and Foundations, **63**(5): 101363. doi:10.1016/j.sandf.2023.101363.

Church, M. 2006. Bed material transport and the morphology of alluvial river channels. Annual Review of Earth and Planetary Sciences, **34**(1): 325–354. doi:10.1146/annurev.earth.33.092203.122721.

Cundall, P.A. 1988. Computer simulations of dense sphere assemblies. *In* Studies in applied mechanics. Vol. 20. Elsevier. pp. 113–123.

Da Cruz, F., Emam, S., Prochnow, M., Roux, J.-N., and Chevoir, F. 2005. Rheophysics of dense granular materials: discrete simulation of plane shear flows. Physical Review E, **72**(2): 21309.

de Bono, J.P., and McDowell, G.R. 2018. Micro mechanics of the critical state line at high stresses. Computers and Geotechnics, **98**: 181–188.

Deyun, L., Catherine, O., and H., C.J.A. 2022. Use of combined static and dynamic testing to quantify the participation of particles in stress transmission. Journal of Geotechnical and Geoenvironmental Engineering, **148**(11): 4022100. doi:10.1061/(ASCE)GT.1943-5606.0002902.

Gong, J., Liu, J., and Cui, L. 2019a. Shear behaviors of granular mixtures of gravel-shaped coarse and spherical fine particles investigated via discrete element method. Powder Technology, **353**: 178–194. doi:10.1016/j.powtec.2019.05.016.

Gong, J., Wang, X., Li, L., and Nie, Z. 2019b. DEM study of the effect of fines content on the small-strain stiffness of gap-graded soils. Computers and Geotechnics, **112**: 35–40. doi:10.1016/j.compgeo.2019.04.008.

Hu, Z., Zhang, Y., and Yang, Z. 2020. Suffusion-induced evolution of mechanical and microstructural properties of gap-graded soils using CFD-DEM. Journal of Geotechnical and Geoenvironmental Engineering, **146**(5): 4020024. doi:10.1061/(ASCE)GT.1943-5606.0002245.

Huang, X. 2014. Exploring critical-state behaviour using DEM. Imperial College London, London.

Kuwano, R., and Jardine, R.J. 2002. On the applicability of cross-anisotropic elasticity to granular materials at very small strains. Géotechnique, **52**(10): 727–749.

Lade, P.V., and Yamamuro, J.A. 1997. Effects of nonplastic fines on static liquefaction of sands. Canadian Geotechnical Journal, **34**(6): 918–928. doi:10.1139/t97-052.

Lade, P.V., Liggio, C.D., and Yamamuro, J.A. 1998. Effects of non-plastic fines on minimum and maximum void ratios of sand. Geotechnical Testing Journal, **21**(4): 336–347. doi:10.1520/GTJ11373J.

Liang, Y., Yeh, T.-C.J., Zha, Y., Wang, J., Liu, M., and Hao, Y. 2017. Onset of suffusion in gap-graded soils under upward seepage. Soils and Foundations, **57**(5): 849–860. doi:10.1016/j.sandf.2017.08.017.

Liu, D. 2022. The influence of particle size distribution on measures of states for granular materials and implications for small strain stiffness. Imperial College London.

Liu, D., and Lourenço, S.D.N. 2021. Stress-dilatancy behaviour of a polymer-coated sand. Acta Geotechnica, **16**(2): 647–652. doi:10.1007/s11440-020-01022-7.

Liu, D., Lourenço, S.D.N., and Yang, J. 2019a. Critical state of polymer-coated sands. Géotechnique, **69**(9): 841–846. doi:10.1680/jgeot.18.P.015.

Liu, D., Sandeep, C.S., Senetakis, K., Nardelli, V., and Lourenço, S.D.N. 2019b. Micromechanical behaviour of a polymer-coated sand. Powder Technology, **347**: 76–84. doi:10.1016/j.powtec.2019.02.030.

Liu, D., O'Sullivan, C., and Carraro, J.A.H. 2021. Influence of particle size distribution on the proportion of stress-transmitting particles and implications for measures of soil State. Journal of Geotechnical and Geoenvironmental Engineering, **147**(3): 4020182. doi:10.1061/(ASCE)GT.1943-5606.0002466.

Liu, D., Morimoto, T., Carraro, J.A.H., and O'Sullivan, C. 2022. A semi-empirical re-evaluation of the influence of state on elastic stiffness in granular materials. Granular Matter, **24**(2): 56. doi:10.1007/s10035-022-01215-9.

Liu, D., Wang, M., and Wang, C. 2024a. Discrete element analyses of stiffness distribution of gap-graded soils with particle property disparity. Journal of Rock Mechanics and Geotechnical Engineering, **17**(4): 2603–2618. doi:10.1016/j.jrmge.2024.05.037.

Liu, D., Yin, Z.-Y., and O'Sullivan, C. 2025. DEM exploration of stress transmission and small strain behavior of rubber sand mixtures. Journal of Geotechnical and Geoenvironmental Engineering, **151**(5): 4025031. doi:10.1061/JGGEFK.GTENG-12823.

Liu, D., Zhao, J., Feng, S., and Chen, H. 2026a. The role of particle shape in stress transmission and stiffness in gap-graded soils. Computers and Geotechnics, **192**: 107857. doi:10.1016/j.compgeo.2025.107857.

Liu, D., Lyu, M.-Z., and Zhao, J. 2026b. Quantifying the impact of the inherent coupling of particle-scale variability on granular soil behavior: a micromechanical study. Journal of Geotechnical and Geoenvironmental Engineering, **152**(2): 4025181. doi:10.1061/JGGEFK.GTENG-14000.

Liu, D., O'Sullivan, C., and Carraro, J.A.H. 2023. The influence of particle size distribution on the stress distribution in granular materials. Géotechnique, **73**(3): 250–264. doi:10.1680/jgeot.21.00127.

Liu, D.-Y., and Lyu, M.-Z. 2023. Uncertainty quantification for granular materials with a stochastic discrete element method. Computers and Geotechnics, **161**: 105560. doi:10.1016/j.compgeo.2023.105560.

Liu, D.-Y., and Lyu, M.-Z. 2024. Capturing the random mechanical behavior of granular materials: a comprehensive stochastic discrete element method study. Géotechnique, 1–35.

Liu, D.-Y., Wang, C., and Lyu, M.-Z. 2024b. Elucidating the complexity of stress interactions in polymer-coated granular materials via copula-based probabilistic dependence configurations. Powder Technology, **435**: 119405. doi:10.1016/j.powtec.2024.119405.

Liu, D.-Y., Wang, M.-T., and Wang, C. 2024c. Evaluation of mechanical behaviour of gap-graded soils with particle property disparity. Computers and Geotechnics, **167**: 106099. doi:10.1016/j.compgeo.2024.106099.

Love, A.E.H. 2013. A treatise on the mathematical theory of elasticity. Cambridge University Press.

Minh, N.H., Cheng, Y.P., and Thornton, C. 2014. Strong force networks in granular mixtures. Granular Matter, **16**(1): 69–78. doi:10.1007/s10035-013-0455-3.

Mitchell, J.K., and Soga, K. 1976. Fundamentals of soil behavior. John Wiley & Sons. Inc., New York. p. 422.

Murthy, T.G., Loukidis, D., Carraro, J. A. H., Prezzi, M., and Salgado, R. 2007. Undrained monotonic response of clean and silty sands. Géotechnique, **57**(3): 273–288. doi:10.1680/geot.2008.58.6.536.

Nardelli, V., and Coop, M.R. 2019. The experimental contact behaviour of natural sands: normal and tangential loading. Géotechnique, **69**(8): 672–686. doi:10.1680/jgeot.17.P.167.

Nardelli, V., Coop, M. R., Andrade, J. E., and Paccagnella, F. 2017. An experimental investigation of the micromechanics of Eglin sand. Powder Technology, **312**: 166–174. doi:10.1016/j.powtec.2017.02.009.

Ni, Q., Tan, T. S., Dasari, G. R., and Hight, D. W. 2004. Contribution of fines to the compressive strength of mixed soils. Géotechnique, **54**(9): 561–569.

Otsubo, M. 2016. Particle scale analysis of soil stiffness and elastic wave propagation. Ph.D. thesis, Imperial College London, London.

Otsubo, M., Kuwano, R., O'Sullivan, C., and Shire, T. 2021. Using geophysical data to quantify stress transmission in gap-graded granular materials. Géotechnique, 1–18.

Potyondy, D.O., and Cundall, P.A. 2004. A bonded-particle model for rock. International Journal of Rock Mechanics and Mining Sciences, **41**(8 SPEC.ISS.): 1329–1364. doi:10.1016/j.ijrmms.2004.09.011.

Rahman, M.M., Lo, S.R., and Gnanendran, C.T. 2008. On equivalent granular void ratio and steady state behaviour of loose sand with fines. Canadian Geotechnical Journal, **45**(10): 1439–1456. doi:10.1139/T08-064.

Salgado, R., Bandini, P., and Karim, A. 2000. Shear strength and stiffness of silty sand. Journal of Geotechnical and Geoenvironmental Engineering, **126**(5): 451–462. doi:10.1061/(ASCE)1090-0241(2000)126:5(451).

Sandeep, C.S., and Senetakis, K. 2018. Grain-scale mechanics of quartz sand under normal and tangential loading. Tribology International, **117**: 261–271. doi:10.1016/j.triboint.2017.09.014.

Sandeep, C.S., He, H., and Senetakis, K. 2018. An experimental micromechanical study of sand grain contacts behavior from different geological environments. Engineering Geology, **246**: 176–186. doi:10.1016/j.enggeo.2018.09.030.

Senetakis, K., and Sandeep, C.S. 2017. Experimental study of sand grains behavior at their contacts with force- and displacement-controlled sliding tests. Underground Space, **2**(1): 38–44. doi:10.1016/j.undsp.2017.03.001.

Shen, C.K. 1977. The effect of fines on liquefaction of sands. Proceedings of the 9th ICSMFE. Vol. 2. pp. 381–385

Shipton, B., and Coop, M.R. 2015. Transitional behaviour in sands with plastic and non-plastic fines. Soils and Foundations, **55**(1): 1–16. doi:10.1016/j.sandf.2014.12.001.

Shire, T. 2014. Micro-scale modelling of granular filters. PhD thesis, Imperial College London, London, UK.

Shire, T., O'Sullivan, C., Hanley, K.J., and Fannin, R.J. 2014. Fabric and effective stress distribution in internally unstable soils. Journal of Geotechnical and Geoenvironmental Engineering, **140**(12): 04014072. doi:10.1061/(ASCE)GT.1943-5606.0001184.

Shire, T., O'Sullivan, C., and Hanley, K.J. 2016. The influence of fines content and size-ratio on the micro-scale properties of dense bimodal materials. Granular Matter, **18**(3).

Song, S., Wang, P., Yin, Z., and Cheng, Y.P. 2024. Micromechanical modeling of hollow cylinder torsional shear test on sand using discrete element method. Journal of Rock Mechanics and Geotechnical Engineering, **16**(12): 5193–5208. doi:10.1016/j.jrmge.2024.02.010.

Sufian, A., Artigaut, M., Shire, T., and O'Sullivan, C. 2021. Influence of fabric on stress distribution in gap-graded soil. Journal of Geotechnical and Geoenvironmental Engineering, **147**(5): 4021016. doi:10.1061/(ASCE)GT.1943-5606.0002487.

Thevanayagam, S. 2000. Liquefaction potential and undrained fragility of silty sands. Proceedings of the 12th International Conference on Earthquake Engineering, 2383.

Thevanayagam, S., Shenthan, T., Mohan, S., and Liang, J. 2002. Undrained fragility of clean sands, silty sands, and Sandy Silts. Journal of Geotechnical and Geoenvironmental Engineering, **128**(10): 849–859. doi:10.1061/(ASCE)1090-0241(2002)128:10(849).

Thompson, A.P., Aktulga, H.M., Berger, R., Bolintineanu, D.S., Brown, W.M., Crozier, P.S., et al. 2022. LAMMPS—a flexible simulation tool for particle-based materials modeling at the atomic, meso, and continuum scales. Computer Physics Communications, **271**: 108171.

Thornton, C. 2000. Numerical simulations of deviatoric shear deformation of granular media. Géotechnique, **50**(1): 43–53.

Tian, Y., and Senetakis, K. 2022. On the contact problem of soft-rigid interfaces: incorporation of Mindlin–Deresiewicz and self-deformation concepts. Granular Matter, **24**(1): 28. doi:10.1007/s10035-021-01186-3.

Tian, Y., and Senetakis, K. 2024. On the creep problem of soft-rigid interfaces: analysis of the normal contact behavior and application of creep models. Granular Matter, **26**(1): 8. doi:10.1007/s10035-023-01377-0.

Wang, P., Yin, Z.Y., Hicher, P.Y., and Cui, Y.-J. 2023. Micro-mechanical analysis of one-dimensional compression of clay with DEM. International Journal for Numerical and Analytical Methods in Geomechanics, **47**(15): 2706–2724. doi:10.1002/nag.3597.

Wang, P., Xu, C., Yin, Z.-Y., Song, S., Xu, C., and Dai, S. 2024. A DEM-based generic modeling framework for hydrate-bearing sediments. Computers and Geotechnics, **171**: 106287. doi:10.1016/j.compgeo.2024.106287.

Weber, J. 1966. Recherches concernant les contraintes intergranulaires dans les milieux pulvérulents. Bulletin de Liaison Des Ponts-et-Chaussées, **20**: 1–20.

Xu, L., and Coop, M.R. 2017. The mechanics of a saturated silty loess with a transitional mode. Géotechnique, **67**(7): 581–596.

Yang, J., and Liu, X. 2016. Shear wave velocity and stiffness of sand: the role of non-plastic fines. Géotechnique, **66**(6): 500–514.

Yang, J., Wei, L. M., and Dai, B. B. 2015. State variables for silty sands: global void ratio or skeleton void ratio? Soils and Foundations, **55**(1): 99–111. doi:10.1016/j.sandf.2014.12.008.

Yang, J., Liu, X., Rahman, M.M., Lo, R., Goudarzy, M., and Schanz, T. 2018. Shear wave velocity and stiffness of sand: the role of non-plastic fines. Géotechnique, **68**(10): 931–934. doi:10.1680/jgeot.16.d.006.

Zhao, J., Zhao, S., and Luding, S. 2023. The role of particle shape in computational modelling of granular matter. Nature Reviews Physics, 1–21.

Zhao, S., Evans, T. M., and Zhou, X. 2018. Effects of curvature-related DEM contact model on the macro- and micro-mechanical behaviours of granular soils. Géotechnique, **68**(12): 1085–1098. doi:10.1680/jgeot.17.P.158.

Zuo, L., and Baudet, B.A. 2015. Determination of the transitional fines content of sand-non plastic fines mixtures. Soils and Foundations, **55**(1): 213–219. doi:10.1016/j.sandf.2014.12.017.